The ESCRT-Related CHMP1A and B Proteins Mediate Multivesicular Body Sorting of Auxin Carriers in *Arabidopsis* and Are Required for Plant Development [W]

Christoph Spitzer, Francisca C. Reyes, Rafael Buono, Marek K. Sliwinski,[1] Thomas J. Haas,[2] and Marisa S. Otegui[3]

Department of Botany, University of Wisconsin, Madison, Wisconsin 53706

Plasma membrane proteins internalized by endocytosis and targeted for degradation are sorted into lumenal vesicles of multivesicular bodies (MVBs) by the endosomal sorting complexes required for transport (ESCRT) machinery. Here, we show that the *Arabidopsis thaliana* ESCRT-related CHARGED MULTIVESICULAR BODY PROTEIN/CHROMATIN MODIFYING PROTEIN1A (CHMP1A) and CHMP1B proteins are essential for embryo and seedling development. Double homozygous *chmp1a chmp1b* mutant embryos showed limited polar differentiation and failed to establish bilateral symmetry. Mutant seedlings show disorganized apical meristems and rudimentary true leaves with clustered stomata and abnormal vein patterns. Mutant embryos failed to establish normal auxin gradients. Three proteins involved in auxin transport, PINFORMED1 (PIN1), PIN2, and AUXIN-RESISTANT1 (AUX1) mislocalized to the vacuolar membrane of the mutant. PIN1 was detected in MVB lumenal vesicles of control cells but remained in the limiting membrane of *chmp1a chmp1b* MVBs. The *chmp1a chmp1b* mutant forms significantly fewer MVB lumenal vesicles than the wild type. Furthermore, CHMP1A interacts in vitro with the ESCRT-related proteins At SKD1 and At LIP5. Thus, *Arabidopsis* CHMP1A and B are ESCRT-related proteins with conserved endosomal functions, and the auxin carriers PIN1, PIN2, and AUX1 are ESCRT cargo proteins in the MVB sorting pathway.

INTRODUCTION

Endosomes are membrane-bound organelles that can be classified based on their main functions into four categories: early, recycling, intermediate, and late endosomes. The first endosomal compartments that receive endocytosed cargo from the plasma membrane are early endosomes. Early and recycling endosomes recycle endocytosed plasma membrane proteins back to the plasma membrane. These endosomes mature into intermediate and late endosomes (also called multivesicular bodies [MVBs]), which have two major sorting functions: the recycling of vacuolar cargo receptors back to the *trans* Golgi network and the sorting of membrane proteins for degradation (Gruenberg and Stenmark, 2004; Russell et al., 2006). Membrane proteins targeted for degradation are sequestered into lumenal vesicles that arise from invaginations of the endosomal membrane. When the late endosomes or MVBs fuse with the lysosome/vacuole, the lumenal vesicles are released into the vacuolar lumen and degraded (Piper and Katzmann, 2007). In addition, late endosomes also mediate the transport of newly synthesized vacuolar proteins from the Golgi to the vacuole. Thus, endosomes are key sorting organelles that contribute to the regulation of the protein composition of the plasma membrane, the *trans* Golgi network, and the vacuoles/lysosomes.

Plants exhibit a highly dynamic endosomal system (recently reviewed in Muller et al., 2007; Robinson et al., 2008; Spitzer and Otegui, 2008). In the last decade, particular attention has been paid to the endosomal recycling and vesicular trafficking of plant plasma membrane proteins involved in auxin transport, such as the PINFORMED (PIN) proteins and AUXIN-RESISTANT1 (AUX1) (Geldner et al., 2001; Muday et al., 2003; Abas et al., 2006; Kleine-Vehn et al., 2006, 2008b; Sieburth et al., 2006; Dhonukshe et al., 2007; Robert et al., 2008). Many PIN proteins show polarized distribution, either in the basal or apical part of the cell, consistent with their function in polar auxin transport. PIN1 is involved in auxin efflux from the cytoplasm and seems to be constitutively recycled from endosomes in a pathway dependent on GNOM (Geldner et al., 2003), a GDP/GTP exchange factor (GEF) for the ADP-ribosylation factor (ARF) GTPases (Steinmann et al., 1999), likely localized to recycling endosomes (Geldner et al., 2003). Interestingly, the recycling of not all auxin carriers seems to be mediated by GNOM. For example, the auxin influx carrier AUX1 is recycled from endosomes to the plasma membrane in a GNOM-independent manner (Kleine-Vehn et al., 2006). Other endosomal components, such as *Arabidopsis thaliana* homologs of the RAB5 GTPases (RABF2A/RHA1 and RABF2B/ARA7) and the retromer complex, which in yeast and animals mediates endosome-to-*trans* Golgi network recycling, also affect trafficking of PIN proteins (Jaillais et al., 2006, 2007; Dhonukshe et al., 2008; Kleine-Vehn et al., 2008a). Degradation

of PIN proteins has been suggested to depend on proteosome activity or on vacuolar degradation (Abas et al., 2006; Kleine-Vehn et al., 2008a; Laxmi et al., 2008). However, the mechanism regulating the turnover and degradation of PIN and other auxin carriers is not known.

In fact, almost nothing is known about endosomal sorting of plant plasma membrane proteins for degradation, and not even one plasma membrane protein has been identified as cargo for MVB lumenal vesicles in plants. The vesiculation process operating in MVBs is highly regulated and involves the recognition and sorting of plasma membrane proteins that are to be degraded. In yeast and animal cells, ubiquitination of membrane proteins acts as a signal for both endocytosis and sorting into MVB lumenal vesicles (Katzmann et al., 2001; Hicke and Dunn, 2003). Both the formation of MVBs and the recognition of ubiquitinated cargo proteins depend on a group of cytoplasmic proteins called Class E vacuolar sorting proteins (VPS), which form multimeric complexes called endosomal sorting complexes required for transport (ESCRTs). When the ubiquitinated membrane proteins reach the endosomes, a first complex called Vps27/Hse1 (Hbp, STAM, and EAST 1) (also named ESCRT-0) is recruited from the cytoplasm to the endosomes by interacting with phosphatidylinositol 3-phosphate, which is abundant in endosomal membranes, and with the ubiquitin on the cargo membrane proteins (Katzmann et al., 2003). Subsequently, three more complexes, called ESCRT-I, -II, and -III, are recruited to the endosomal membrane (Katzmann et al., 2002, 2003; Bowers et al., 2004; Babst, 2005; Hurley and Emr, 2006; Nickerson et al., 2007; Teis et al., 2008). Once the ESCRTs are assembled on the endosomal membrane, the ubiquitin molecules are removed from the cargo proteins by the ubiquitin hydrolase DEGRADATION OF ALPHA 4 (Richter et al., 2007). The dissociation of the ESCRTs from the endosomal membrane depends on another class E VPS protein, the AAA (ATPases Associated with various cellular Activities) ATPase Vps4p/SKD1 (for SUPPRESSOR OF K$^+$ TRANSPORT GROWTH DEFECT1) (Babst et al., 1997, 1998). Studies in yeast, mammalian, and plant cells have shown that expression of dominant-negative versions of Vps4p/SKD1 causes ESCRT components to accumulate in membrane-bound complexes and compromises lumenal vesicle formation (Babst et al., 1998; Yoshimori et al., 2000; Lin et al., 2005; Haas et al., 2007). It is important to note that ubiquitin recognition is not the only mechanism for MVB sorting since nonubiquitinated transmembrane proteins, such as yeast Sna3, are also sorted into MVB internal vesicles (Reggiori and Pelham, 2001).

The modulation of Vps4p/SKD1 ATPase activity and its association with endosomes are mediated by accessory proteins, such as CHMP1/Did2p (CHARGED MULTIVESICULAR BODY PROTEIN/CHROMATIN MODIFYING PROTEIN1), LIP5/Vta1p (LYST-INTERACTING PROTEIN 5/VPS TWENTY ASSOCIATED1 PROTEIN), and Vps60p/CHMP5 (Yeo et al., 2003; Scott et al., 2005a, 2005b; Azmi et al., 2006, 2008; Nickerson et al., 2006; Vajjhala et al., 2007). Did2p in yeast is required for ESCRT-III dissociation from endosomal membranes and directly interacts with the microtubule interacting domain (MIT) of Vps4p/SKD1 via its C-terminal MIT-interacting motive (MIM domain) (Scott et al., 2005a; Obita et al., 2007). Interestingly, human CHMP1 also contains a functional bipartite nuclear localization signal, regu-

lates gene transcription, and acts as a tumor suppressor in humans (Stauffer et al., 2001; Li et al., 2008). In addition, just like other ESCRT components, CHMP1 is localized to the midbody and is necessary for completion of animal cytokinesis (Yang et al., 2008).
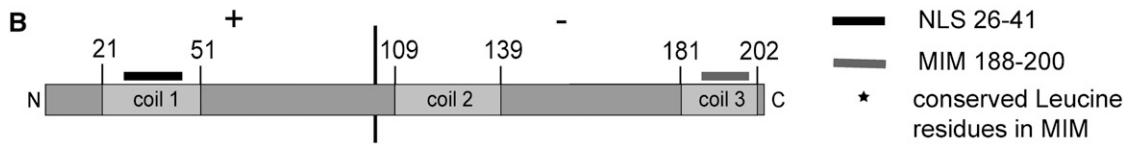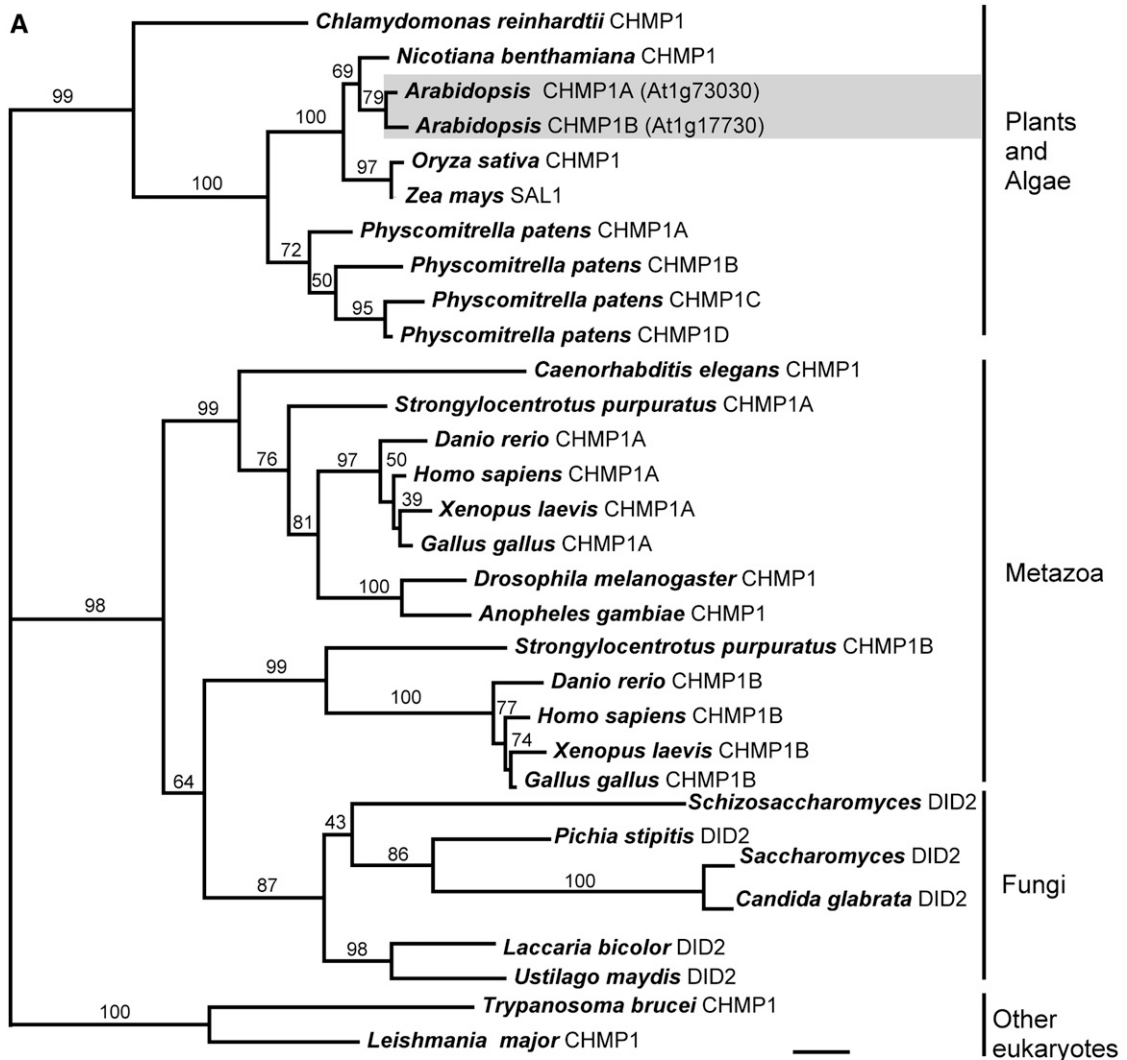
Putative homologs of all the main ESCRT and ESCRT-related proteins with the exception of the Vps27/Hse1p components, have been identified in plants (Mullen et al., 2006; Spitzer et al., 2006; Winter and Hauser, 2006; Leung et al., 2008). However, only the endosomal functions of a few of these proteins, such as the ESCRT-I component ELCH and the ESCRT-related proteins SKD1, LIP5/Vta1p, and CHMP1/Did2p (Doa4-Independent Degradation 2) have been studied to date in plants. Two putative plant *DID2/CHMP1* homologs, *SUPERNUMERARY ALEURONE LAYER1* (*SAL1*) in maize (*Zea mays*) (Shen et al., 2003) and *CHMP1* in *Nicotiana benthamiana* (Yang et al., 2004), have been identified. The maize SAL1 protein localizes to MVBs, and a *sal1* knockdown mutant shows abnormal aleurone (epidermal endosperm layer) differentiation, likely due to alterations in the trafficking of plasma membrane proteins that are key regulators of aleurone cell fate specification (Tian et al., 2007). The *Arabidopsis* genome encodes two CHMP1 proteins, CHMP1A and B, which are similar in sequence and domain structure to mammalian CHMP1 and yeast Did2p.

In this study, we report that the *Arabidopsis* CHMP1 proteins are essential for embryo development and that the *chmp1a chmp1b* double mutant dies before or shortly after germination. Mutant cells are able to form MVBs, although these contain fewer lumenal vesicles compared with those of the wild type. We show that the auxin carriers PIN1, PIN2, and AUX1 are cargo of the ESCRT machinery and that the ability to sort MVB cargo into lumenal vesicles is compromised in mutant cells.

RESULTS

CHMP1A and B Are Similar to Yeast Did2p and Mammalian CHMP1

Putative *DID2/CHMP1* orthologs are found in all eukaryotic organisms sequenced so far. Whereas most metazoans are characterized by the presence of two *CHMP1* genes (*CHMP1A* and *CHMP1B*), fungi and most higher plants contain only one *CHMP1* copy (Figure 1A; see Supplemental Figure 1 and Supplemental Data Set 1 online). The *Arabidopsis* genome contains two putative *DID2/CHMP1* gene copies, *CHMP1A* (At1g73030) and *CHMP1B* (At1g17730), which encode proteins that are 95% identical to each other and are expressed in all organs (Genevestigator; https://www.genevestigator.ethz.ch). Several features of the two *Arabidopsis* CHMP1 proteins support the idea that they are in fact the counterparts of yeast Did2p and mammalian CHMP1A/B. First, the amino acid charge distribution, with a positively charged N-terminal domain and a negatively charged C-terminal domain, is characteristic of Did2p/CHMP1 and other ESCRT-III and ESCRT III–related proteins. Second, *Arabidopsis* CHMP1 proteins contain a putative MIM domain that has been shown to mediate the interaction between human CHMP1A and Vps4p/SKD1 (Scott et al., 2005a; Stuchell-Brereton et al., 2007)

Figure 1. Characterization of *Arabidopsis* CHMP1 Protein Structure and Phylogeny of CHMP1 Proteins in Eukaryotes.

(A) Phylogenetic analysis of CHMP1-related proteins from plants, animals, fungi, and other organisms using RAxML. The bootstrap values are shown

(Figures 1B and 1C). Third, both *Arabidopsis* proteins are predicted to contain three coiled-coil domains just like mammalian CHMP1A/B and Did2p (prediction made by using Lupas' algorithm; Lupas et al., 1991). Fourth, *Arabidopsis* CHMP1A and B are very similar in size (203 amino acids) compared with yeast Did2p (204 amino acids) and human CHMP1A and B (196 amino acids). No additional plant-specific motives that would suggest additional or diverged functions have been detected in the *Arabidopsis* CHMP1 proteins.

Arabidopsis CHMP1A Interacts with SKD1 and LIP5

To determine if the *Arabidopsis* CHMP1 proteins are in fact part of the ESCRT machinery in plants, we performed interaction assays between CHMP1A and other known ESCRT-associated proteins. We expressed recombinant At CHMP1A, At SKD1, and At LIP5 tagged with either glutathione *S*-transferase (GST) or 6xHIS in bacteria and tested for interactions. Although the recombinant tagged CHMP1A proteins tend to degrade quickly under the binding assay conditions, we confirmed that CHMP1A interacts with both SKD1 and LIP5 (Figures 2A and 2B), as has been reported for yeast Did2p (Scott et al., 2005a; Lottridge et al., 2006; Nickerson et al., 2006; Tsang et al., 2006; Vajjhala et al., 2006), further supporting the involvement of the *Arabidopsis* CHMP1 proteins in ESCRT-mediated MVB sorting.

The *chmp1a chmp1b* Double Mutant Shows Embryo Development Defects

To gain insights into *Arabidopsis* CHMP1 function, we identified T-DNA insertion lines for *CHMP1A* and *B*. We isolated two mutant alleles, *chmp1a-1* (SAIL_580_C03) and *chmp1b-1* (SALK_135944), each of which contains an insertion in the first exon (Figure 2C). Sequencing of the insertion sites confirmed integration of the T-DNA insertion 95 bp downstream of the start codon of *CHMP1A* and 220 bp downstream of the start codon of *CHMP1B*. We could not amplify full-length transcripts of either *CHMP1A* or *B* by RT-PCR in the homozygous T-DNA lines of the corresponding genes, indicating that both T-DNA insertions efficiently disrupt gene transcription (Figure 2D).

We analyzed the number of cotyledons (see Supplemental Figure 2A online), leaf development, flowering time, flower structure, and seeds per siliques and found no differences between the single *chmp1* mutants and wild-type control plants. The high sequence similarity between the two *CHMP1* gene products and their similar expression pattern suggest that they may have redundant functions. We therefore crossed both single mutants

and attempted to identify double homozygous mutant plants by PCR-based genotyping. The analysis of 111 T3 plants produced by self-pollinated *CHMP1A/chmp1a; chmp1b/chmp1b* plants yielded 35 *CHMP1A/CHMP1A chmp1b/chmp1b* plants and 76 *CHMP1A/chmp1a chmp1b/chmp1b* plants; however, no homozygous double mutant plants were identified. Similar numbers were obtained for the T3 generation from self-pollinated *chmp1a/chmp1a CHMP1B/chmp1b* plants (Table 1). Interestingly, mutant plants containing just one wild-type allele of either *CHMP1A* or *CHMP1B* were completely normal. The observed segregation ratios suggest lethality at either embryo or seedling stage and led us to analyze the seeds from these plants. We found that 21.4% (SD ± 4.9; n = 39 siliques) of the seeds from *CHMP1A/chmp1a chmp1b/chmp1b* plants and 23.4% (SD ± 4.6; n = 40 siliques) of the seeds from *chmp1a/chmp1a CHMP1B/chmp1b* plants were paler than normal seeds, whereas only 2.7% (SD ± 2.1; n = 28 siliques) of the seeds in wild-type plants had abnormal appearance (Figures 2E and 2F). The abnormal seeds in mutant siliques contained embryos that ranged from ball-like structures to cone-shaped embryos with a stunted axis and multiple, rudimentary cotyledons. We confirmed that these abnormal embryos were the *chmp1a chmp1b* double homozygous mutants by PCR-based genotyping (see Supplemental Figure 2B online). In addition, we performed a protein gel blot of proteins extracted from *chmp1a chmp1b* and wild-type embryos using polyclonal antibodies raised against the maize SAL1/CHMP1 protein (Tian et al., 2007). Whereas a strong band of ∼27 kD corresponding to CHMP1 was identified in wild-type protein extracts, only a very faint band of similar size was detected in the mutant (Figure 2G). Either the double mutant embryos are able to synthesize small amounts of CHMP1 or a small amount of maternal material tissue was carried over during the isolation of embryos. In addition, no bands of smaller molecular sizes that could correspond to truncated CHMP1 fragments were detected in the mutant protein extracts.

The incorporation of a genomic fragment containing the *CHMP1B* gene into *CHMP1A/chmp1a chmp1b/chmp1b* plants fully rescued the defective embryo phenotype in the double homozygous mutant, further confirming that the phenotypic embryo alterations were due to the T-DNA insertions in the *CHMP1* genes (see Supplemental Figure 2C online).

The *Arabidopsis* CHMP1A and B Proteins Are Required for Embryonic Axis Establishment and Seedling Growth

To understand the function of the CHMP1A and B proteins in plant development, we studied the phenotypic alterations of the

---

Figure 1. (continued).

above each branch. The accession numbers and gene identifiers for the sequences used in this analysis are provided in Methods. Scale indicates 0.1 amino acid substitutions per site.

(B) Schematic representation of *Arabidopsis* CHMP1A and B proteins. CHMP1A and B differ in 10 amino acid residues from each other. The asymmetric amino acid charge distribution of CHMP1 proteins is indicated by + and − for predominantly basic and acidic amino acid residues, respectively. NLS, nuclear localization signal. Coiled-coil domains were identified with the algorithm from Lupas et al. (1991).

(C) Amino acid alignment of *Arabidopsis* CHMP1A and B, human CHMP1A and B, and yeast Did2p. Black indicates identical residues, and gray represents similar residues. Asterisks indicate conserved leucine residues in the MIM domain.
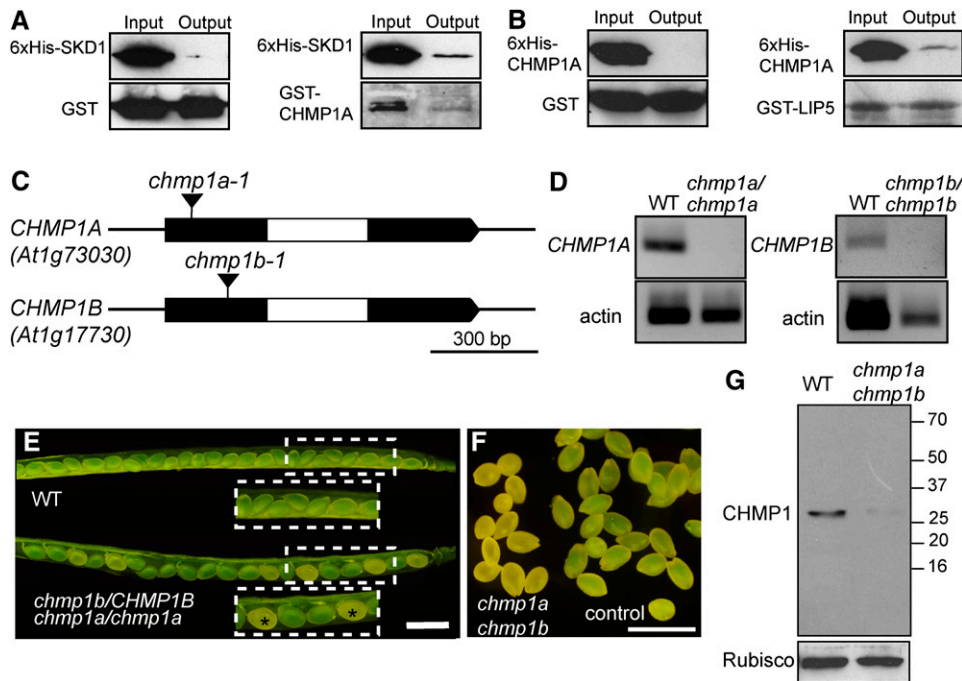
Figure 2. Interaction Analysis between CHMP1 and ESCRT-Related Proteins and Characterization of *Arabidopsis chmp1* Mutant Alleles.

(A) and **(B)** In vitro pull-down assays confirmed the interaction between CHMP1A and SKD1 **(A)** and CHMP1A and LIP5 **(B)**. Protein gel blots of in vitro glutathione agarose pull-down show that 6xHis tagged At-SKD1 interacts with GST-At-CHMP1A but not with GST alone and 6xHis tagged At-CHMP1a interacts with GST-At-LIP5 but not with GST alone. All the recombinant proteins were detected using either anti-GST (bottom panels) or anti-His (top panels) antibodies.

(C) Schematic representation of distribution of exons (black) and introns (white) in *CHMP1A* and *B*. Inverted wedges indicate the T-DNA insertions in the first exon of *CHMP1A* and *CHMP1B*.

(D) RT-PCR from RNA extracts of the *chmp1a* and *chmp1b* single mutants. Two biological replicates were performed.

(E) Seeds from wild-type and *chmp1a/CHMP1A chmp1b/chmp1b* plants. Asterisks indicate double mutant seeds.

(F) Detail of seeds dissected from one single mutant silique showing double mutant and wild type–looking (control) seeds containing two or more *chmp1* mutant alelles.

(G) Protein gel blot of total protein extracts from wild-type and *chmp1a chmp1b* mutant embryos. CHMP1 proteins were detected with a polyclonal antibody raised against the full-length maize SAL1/CHMP1 protein (Tian et al., 2007). Ribulose-1,5-bisphosphate carboxylase/oxygenase (Rubisco) was used as loading control.

Bars = 1 mm.

double homozygous mutant embryos in more detail. In siliques segregating the T-DNA *chmp1a-1* and *chmp1b-1* mutant alleles, the distinction between double *chmp1a chmp1b* mutant and wild type–looking developing embryos first became evident during the heart stage, when the mutant embryos remained globular in shape without differentiating a polar axis (Figures 3A and 3B). By the time that control embryos reached the bent cotyledon and mature embryo stages, most of the *chmp1a chmp1b* embryos were developmentally delayed but had acquired some degree of axial organization. Most mutant embryos developed a variable number of unevenly sized cotyledons (commonly three or four), sometimes partially fused to each others, and a root pole (Figures 3C to 3H). Longitudinal sections of these embryos revealed that the procambial strand seemed to be in an excentric position, which also suggests altered radial symmetry (Figures 3I to 3L).

Few double mutant seeds were able to germinate and grow rudimentary roots, hypocotyls, and leaves (Figure 4). The double mutant seedlings showed slower growth rate than control seed-

lings, multiple cotyledons, and disorganized root and shoot apical meristems. In addition, leaves and cotyledons showed clustered stomata and an altered leaf venation pattern, whereas roots had highly enlarged epidermal cells (Figures 4H to 4M). All double mutant seedlings died a few weeks after germination.

Interestingly, the mutant embryos can be induced to differentiate calli in vitro (Wei et al., 2006) (see Supplemental Figures 2D to 2F online), indicating that the double mutation in the *CHMP1* genes does not compromise directly cell viability.

Auxin Gradients Are Not Properly Established in *chmp1a chmp1b* Embryos and Seedlings

The defective polar axis differentiation and the presence of multiple rudimentary cotyledons in the *chmp1a chmp1b* mutant embryos resemble mutants compromised in auxin transport. To test for auxin-related defects in the double mutant, we introduced a reporter gene that consists of the auxin-responsive

Table 1. Progeny Analysis of Self-Pollinated *Arabidopsis* Plants Segregating the *chmp1a-1* and *chmp1b-1* Mutant Alleles

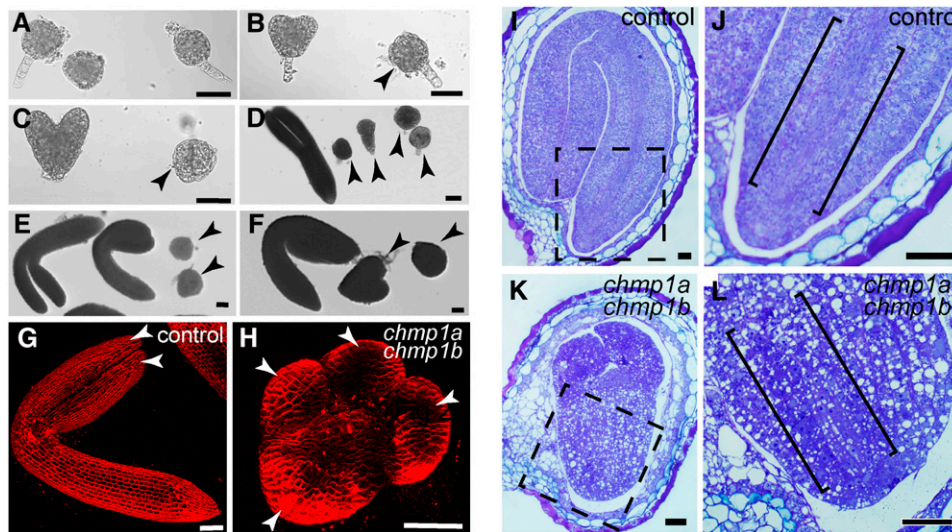|	chmp1a/CHMP1A chmp1b/chmp1b			chmp1a/chmp1a chmp1b/CMP1B		
Genotypes	A/A b-1/b-1	A/a-1 b-1/b-1	a-1/a-1 b-1/b-1	a-1/a-1 B/B	a-1/-1a B/b-1	a-1/a-1 b-1/b-1
Expected	25%	50%	25%	25%	50%	25%
Observed	35 pl (31%)	76 pl (69%)	0 pl (0%)	38 pl (34%)	74 pl (66%)	0 pl (0%)

promoter *DR5rev* driving the expression of green fluorescent protein (*GFP*) (Friml et al., 2003; Ottenschläger et al., 2003) in plants that segregate the *chmp1a-1* and *chmp1b-1* mutant alleles. We established a T3 line homozygous for the *DR5rev_pro:GFP* reporter and compared the GFP signal in control and *chmp1a chmp1b* double mutant embryos isolated from the same silique. As expected, mature control embryos showed strong GFP signal in the embryo root pole and the tips of cotyledons (Friml et al., 2003; Ottenschläger et al., 2003) (Figures 5A to 5C). Mutant embryos displayed strong GFP signal at the root pole and at multiple apical areas. In many cases, more than one GFP-positive area was detected in a mutant cotyledon (Figures 5D and 5E). In other cases, the GFP signal at the apical part of the embryo extended into elongated areas (Figure 5F) and corre-

sponded to embryos with partially fused cotyledons. In contrast with wild-type embryos, mutant embryos also showed a strong signal in procambial strands (Figures 5G and 5I).

PIN1-GFP Is Ectopically Expressed and Mislocalized in the *chmp1a chmp1b* Mutant

We reasoned that the defects in auxin transport in *chmp1a chmp1b* mutant embryos could be related to mislocalization of auxin carriers. We introduced the *PIN1_pro:PIN1-GFP* transgene (Heisler et al., 2005) in *CHMP1A/chmp1a chmp1b/chmp1b* plants and analyzed the expression pattern and subcellular localization of PIN1-GFP in developing embryos. PIN1-GFP expression was restricted to the apical and central region of the globular embryo (Steinmann et al., 1999) and later to the tip of the developing cotyledons and procambial strand (Figures 6A to 6C). In *chmp1a chmp1b* mutants, PIN1-GFP was either ectopically expressed in the entire ball-like embryo or showed a preferential expression in the apical region and the rudimentary cotyledons (Figures 6D to 6F), depending on the developmental stage and severity of the mutant embryo phenotype.

We found that not only PIN1-GFP expression pattern was altered in the mutant but also its subcellular localization. Whereas PIN1-GFP was mostly localized to the plasma membrane in a polarized fashion in control embryos (Steinmann et al., 1999; Geldner et al., 2001) (Figure 6G), PIN1-GFP was found

Figure 3. Phenotypic Analysis of *chmp1a chmp1b* Double Mutant Embryos and Seeds.

(A) to **(F)** Developmental stages of dissected embryos from *chmp1a/chmp1a CHMP1B/chmp1b* plants. Wild type–looking embryos shown on the left side and double mutant embryos (arrowheads) on the right side of panels.

(G) and **(H)** Confocal images of control and mutant embryos. The mutant embryo is seen from a top view showing the presence of four rudimentary cotyledons (arrowheads).

(I) to **(L)** Longitudinal sections of seeds produced by *chmp1a/chmp1a CHMP1B/chmp1b* plants.

(I) and **(J)** Wild type–looking seed used as control.

(J) Detail of the root and procambial strand (indicated by brackets) of the embryo shown in **(I)**.

(K) and **(L)** *chmp1a chmp1b* double mutant embryo.

(L) Detail of the root pole of the mutant embryo shown in **(K)**. Note the excentrically located procambial strand (indicated by brackets).
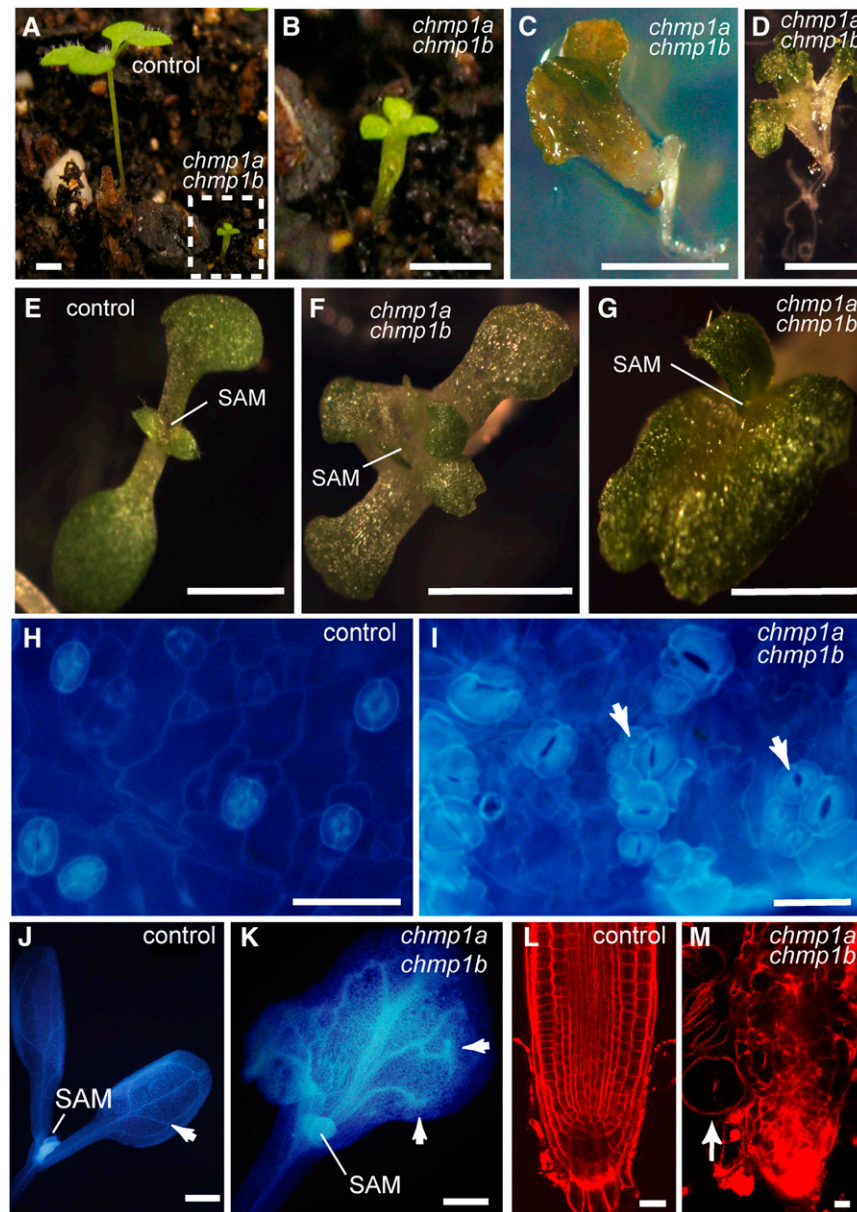
Bars = 50 μm.

Figure 4. Phenotype of *chmp1a chmp1b* Double Mutant Seedlings.

(A) to **(G)** Seedlings derived from *chmp1a/chmp1a CHMP1B/chmp1b* plants. Note multiple cotyledons of mutant seedlings in **(B)** to **(D)**.

(E) to **(G)** Shoot apical regions in control **(E)** and *chmp1a chmp1b* mutant seedlings (**[F]** and **[G]**).

(H) and **(I)** Cotyledons stained with 4',6-diamidino-2-phenylindole showing the distribution of stomata in control **(H)** and mutant seedlings **(I)**. Note the clustered stomata in mutant cotyeldons (arrows in **[I]**).

(J) and **(K)** Seedlings stained with 4',6-diamidino-2-phenylindole showing the venation pattern in cotyledons. Whereas the lateral veins in the control seedlings are fused close to the cotyledon margin (arrow in **[J]**), lateral veins in the mutant cotyledons end freely (arrows in **[K]**). SAM, shoot apical meristem.

(L) and **(M)** Root architecture in control **(L)** and *chmp1a chmp1b* mutant seedlings **(M)** stained with propidium iodide. Note the enlarged root epidermal cells in the mutant (arrow).

Bars = 5 mm in **(A)** to **(D)**, 2 mm in **(E)** to **(G)**, 50 μm in **(H)** and **(I)**, 500 μm in **(J)** and **(K)**, and 20 μm in **(L)** and **(M)**.
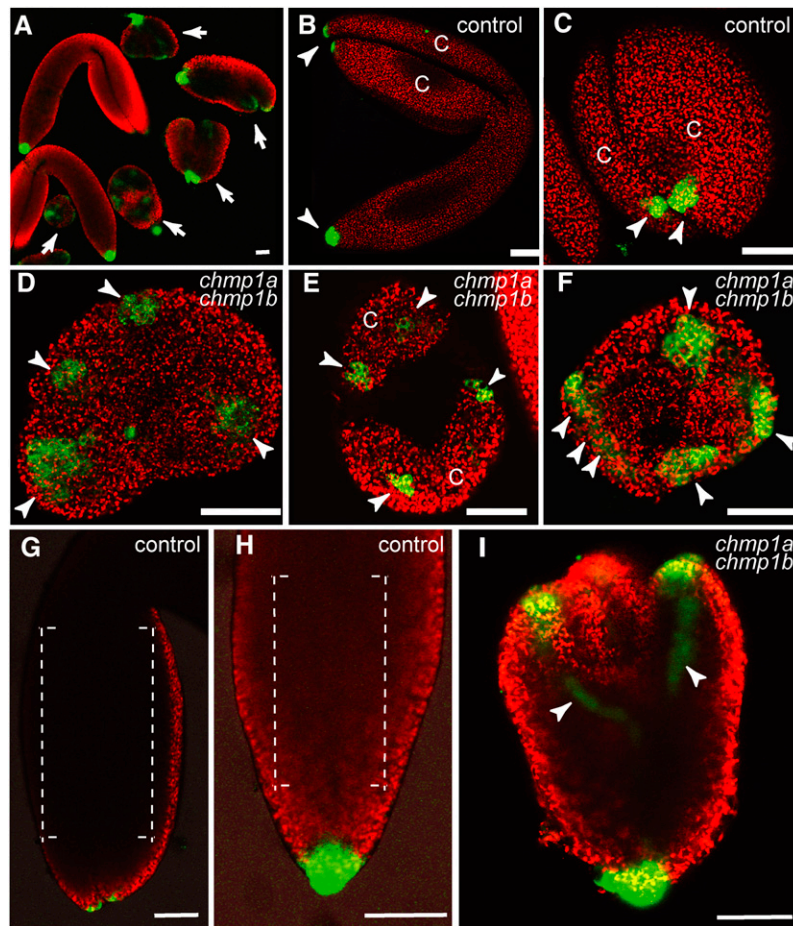
Figure 5. *DR5rev_pro:GFP* Expression in Control and *chmp1a chmp1b* Mutant Embryos.

(A) Overview of wild type–looking (control) and *chmp1a chmp1b* mutant embryos (arrows) expressing the *DR5rev_pro:GFP* reporter. Chlorophyll autofluorescence (red) was used to visualize the embryos.
(B) and **(C)** Control mature embryos. GFP signal (arrowheads) was detected in the tips of cotyledons **(C)** and in the root pole. **(C)** shows detail of apical view of cotyledon.
(D) to **(F)** Optical cross sections through the apical region of double mutant embryos showing GFP signal (arrowheads) in the tip of rudimentary cotyledons **(C)**.
(G) and **(H)** Wild-type embryos with undetectable GFP signal in the procambial strand region (brackets) of cotyledons **(G)** and axis **(H)**.
(I) Double mutant embryo showing strong GFP signal in procambial strands (arrowheads).
Bars = 50 μm.

more uniformly distributed across the plasma membrane, in internal compartments stained by the endocytic dye FM4-64, and at the vacuolar membrane in the *chmp1a chmp1b* homozygous mutant embryos (Figures 6H and 6I).

The localization of the PIN1-GFP protein in the vacuolar membrane of the double mutant cells was confirmed by immunolocalization on cryofixed/freeze-substituted embryos using an antibody against GFP (Figures 7A and 7B).

In addition, when plants were kept in the dark for 24 or 48 h, developing control embryos accumulated PIN1-GFP in the vacuolar lumen (Dhonukshe et al., 2008; Laxmi et al., 2008) but double mutant embryos did not (see Supplemental Figure 3 online), indicating that PIN1-GFP fails to be delivered to the vacuole for degradation in the mutant background.

PIN1 Localizes to MVB Lumenal Vesicles in Control Cells but Not in the *chmp1a chmp1b* Mutant Cells

The accumulation of PIN1-GFP to the vacuolar membrane suggests defective sorting of cargo proteins into MVB lumenal vesicles and impaired subsequent release into the vacuolar lumen. To test this hypothesis, we examined MVBs in high-pressure frozen/freeze-substituted embryos by immunolabeling and electron microscopy. PIN1-GFP signal was found in Golgi stacks, plasma membrane, and MVB lumenal vesicles in control embryos (Figures 8A to 8D). In *chmp1a chmp1b* mutant embryos, most of the PIN1-GFP labeling associated with MVBs was detected on the MVB limiting membrane and not on the lumenal vesicles (Figures 8E to 8G). Control labeling experiments were
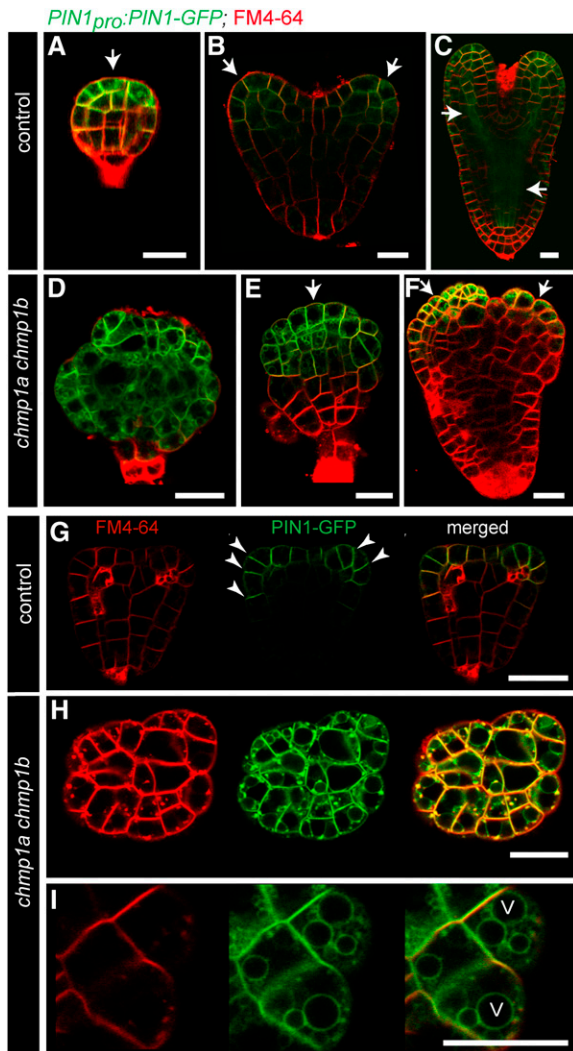
Figure 6. PIN1-GFP Expression and Localization in Control and *chmp1a chmp1b* Mutant Embryos. (Embryos were stained with FM4-64 [red] to visualize the cell outlines.)

(A) to **(C)** Control embryos. Note PIN1-GFP expression at apical/central region (arrow) of a globular stage embryo **(A)**, tips of developing cotyledon (arrows) in heart stage embryo **(B)**, and procambial strands (arrows) of torpedo stage embryo **(C)**.

(D) to **(F)** *chmp1a chmp1b* mutant embryos with altered PIN1-GFP expression pattern. Arrows indicate the areas with higher PIN1-GFP expression.

(G) Control heart stage embryo. PIN1-GFP localizes to the plasma membrane in the emerging cotyledons, predominantly to the apical side of the cells (toward the tip of the cotyledons; arrowheads).

(H) and **(I)** *chmp1a chmp1b* mutant embryo dissected from the same silique used in **(G)**. Note the substantial PIN1-GFP signal from vacuolar membranes and FM4-64–stained compartments. V, vacuole.

Bars = 20 μm.

performed using anti-GFP antibodies on wild-type embryo cells (see Supplemental Figure 4 online).

Although the *chmp1a chmp1b* mutant cells are able to form MVBs, they differ in some general structural features from the control MVBs. We immunolabeled mutant and control samples with antibodies against the plant MVB marker RHA1/RABF2A (Figures 8H to 8J) and conducted a quantitative analysis of labeled MVBs. A statistic analysis of these endosomes indicated that the number of MVB lumenal vesicles per section was reduced significantly in the mutant and that a higher proportion of lumenal vesicles were attached to the MVB limiting membrane compared with control MVBs (Table 2).

AUX1 and PIN2 Are Mislocalized but Not Ectopically Expressed in the *chmp1a chmp1b* Mutant

To test whether other auxin carriers were mislocalized and/or ectopically expressed in the double mutant, we introduced the *AUX1_pro:AUX1-YFP116* (Swarup et al., 2004) and *PIN2_pro:PIN2-GFP* (Laxmi et al., 2008) transgenes in *chmp1a/chmp1a CHMP1B/chmp1b* plants.

In control embryos at the early torpedo stage, AUX1–yellow fluorescent protein (YFP) was strongly expressed at the root pole and procambial strand, whereas ball-shaped mutant embryos from the same siliques showed no detectable expression of AUX1-YFP (Figure 9A, arrows). In mature seeds, both control and double mutant embryos that have acquired some degree of axial organization showed AUX1-YFP signal at the root pole (Figures 9B and 9D). In both control and mutant embryos, AUX1-YFP was localized to the plasma membrane in a nonpolarized fashion. However, in the double mutant embryos, AUX1-YFP was also detected in the vacuolar membrane (Figures 9E and 9F).

In embryos nearing maturity, PIN2-GFP signal was first observed in the adaxial epidermis of cotyledons; however, the overall GFP signal in both mutant and control embryos was very low. Instead, we studied the PIN2-GFP distribution in seedlings. In both double mutant and control roots, the expression of PIN2-GFP was restricted to the epidermis and cortex (Figures 9G and 9H) (Abas et al., 2006), but whereas in control roots most of the PIN2-GFP signal was detected at the apical side (shoot-apex-facing) of epidermal cells in the plasma membrane, in *chmp1a chmp1b* mutant roots, the polarized distribution of PIN2-GFP was partially lost and strong PIN2-GFP signal was also detected in vacuolar membranes (Figures 9I to 9N).

The detection of AUX1-YFP and PIN2-GFP on the vacuolar membrane of mutant cells suggests that AUX1-YFP and PIN2-GFP are also missorted at the MVBs.

Transport of 2S Albumins to the Protein Storage Vacuole Is Not Altered in the *chmp1a chmp1b* Mutant Embryos

Although the general appearance of protein storage vacuoles in the *chmp1a chmp1b* mutant embryos was normal, we wanted to test if the transport of biosynthetic cargo to the vacuole was affected in the mutant embryos. We immunolabeled the seed storage proteins 2S albumins, which have been previously shown to be delivered to the vacuole by MVBs (Otegui et al., 2006) in both cryofixed/freeze-substituted wild-type and mutant
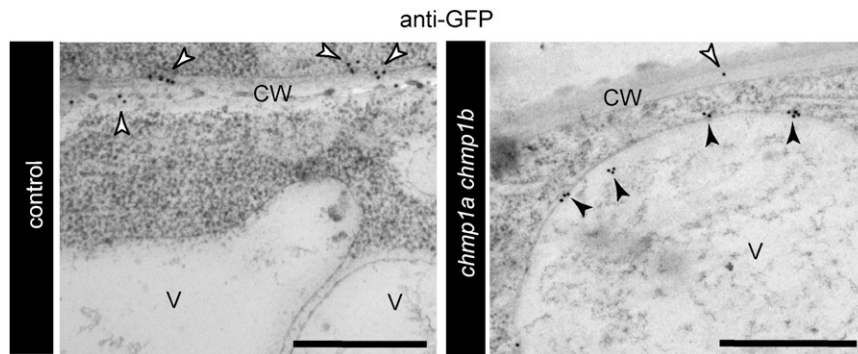
anti-GFP

Figure 7. Immunogold Localization of PIN1-GFP.

Immunogold labeling was performed on high-pressure frozen/freeze-substituted wild type–looking (control) and *chmp1a chmp1b* mutant embryos from self-pollinated *CHMP1A/chmp1a chmp1b/chmp1b/ PIN1_pro:PIN1-GFP/PIN1_pro:PIN1-GFP* plants using polyclonal anti-GFP antibodies. Bars = 500 nm.
(A) Control embryo. GFP signal is detected at the plasma membrane (white arrowheads).
(B) *chmp1a chmp1b* mutant embryos. White arrowheads indicate gold labeling on the plasma membrane and black arrowheads on the vacuolar membrane. CW, cell wall; V, vacuole.

embryos (see Supplemental Figure 5 online). The 2S albumins were detected in Golgi stacks, MVBs, and protein storage vacuoles both in wild-type and mutant samples, indicating that the delivery of this soluble vacuolar cargo is not affected by the *chmp1a chmp1b* mutation.

DISCUSSION

Arabidopsis CHMP1 Is Involved in ESCRT-Dependent MVB Sorting

Comparative genome analyses have shown that the ESCRT machinery (with the exception of the Vps27/Hse1p complex) is conserved in all eukaryotes including plants (Mullen et al., 2006; Spitzer et al., 2006; Winter and Hauser, 2006; Leung et al., 2008). This is supported by recent studies on the ESCRT-I subunit Vps23p/TSG101/ELCH and Vps4p/SKD1 in *Arabidopsis* and in the ice plant *Mesembryanthemum crystallinum*, which confirmed that at least these two plant ESCRT-related proteins have similar biochemical properties and conserved binding partners to those of their yeast and mammalian counterparts (Jou et al., 2006; Spitzer et al., 2006; Haas et al., 2007).

The two *DID2/CHMP1* gene copies that we have identified in *Arabidopsis* encode proteins with characteristic features of ESCRT-III and ESCRT-III–related proteins (including Did2p and Vps60p), such as molecular weight, domain organization, and charge distribution. In yeast, Did2p is recruited to endosomes by its interaction with the Vps2p/Vps24p ESCRT-III subcomplex (Nickerson et al., 2006). Did2p also binds Vps4p/SKD1 and mediates the Vps4p/SKD1-dependent dissociation of ESCRT-III from the endosomal membrane. In addition, Did2p is able to bind both Vta1p/LIP5, which acts as a positive regulator of Vps4p/SKD1 ATPase activity (Azmi et al., 2006, 2008; Lottridge et al., 2006), and IST1, which is assumed to act as a negative regulator of Vps4p/SKD1 (Dimaano et al., 2008; Rue et al., 2008). Therefore, Did2p may have an indirect role in modulating the enzymatic

activity of Vps4/SKD1. In contrast with other ESCRT-related mutants that develop abnormal multistacked endosomes with no vesicles (class E compartments), the *did2Δ* mutant is able to form multivesicular endosomes with enlarged luminal vesicles. However, MVB cargo proteins, such as carboxypeptidase S (a biosynthetic cargo) and Ste3 (a plasma membrane cargo), are missorted in the *did2Δ* mutant, indicating that cargo sorting and MVB vesicle formation are two processes that can be uncoupled (Nickerson et al., 2006).

Just like its yeast and mammalian counterparts, *Arabidopsis* CHMP1A binds At SKD1 and At LIP5 (Figure 2), supporting the high degree of conservation of the ESCRT machinery across eukaryotes. Moreover, the *Arabidopsis chmp1a chmp1b* and the yeast *did2Δ* mutants both missort MVB cargo but are able to form MVB lumenal vesicles. However, in contrast with the *did2Δ* endosomes, the *chmp1a chmp1b* MVBs produced a very low number of lumenal vesicles of normal size. Therefore, whereas Did2p is necessary to sort efficiently MVB cargo into lumenal vesicles but apparently not for lumenal vesicle formation, loss of At CHMP1 prevents MVB lumenal vesicle formation to a large extent. Previous studies have shown structural differences in aberrant endosomes resulting from mutations in homologous ESCRT-related genes in different organisms, suggesting that although the general MVB sorting mechanism is well conserved, some variations are likely to occur among species.

Interestingly, the vacuolar localization of the 2S albumins was not affected in *chmp1a chmp1b* mutant embryos (see Supplemental Figure 4 online), suggesting that the delivery of at least this soluble biosynthetic cargo to the vacuole does not require CHMP1-dependent MVB sorting.

PIN1, PIN2, and AUX1 Are MVB Cargo Proteins in Plants

The mislocalization of PIN1-GFP, PIN2-GFP, and AUX1-YFP to the vacuolar membrane in the *chmp1a chmp1b* mutant strongly support that these proteins are ESCRT cargo and are therefore sorted at MVBs for degradation in the vacuolar lumen (Figure 10).
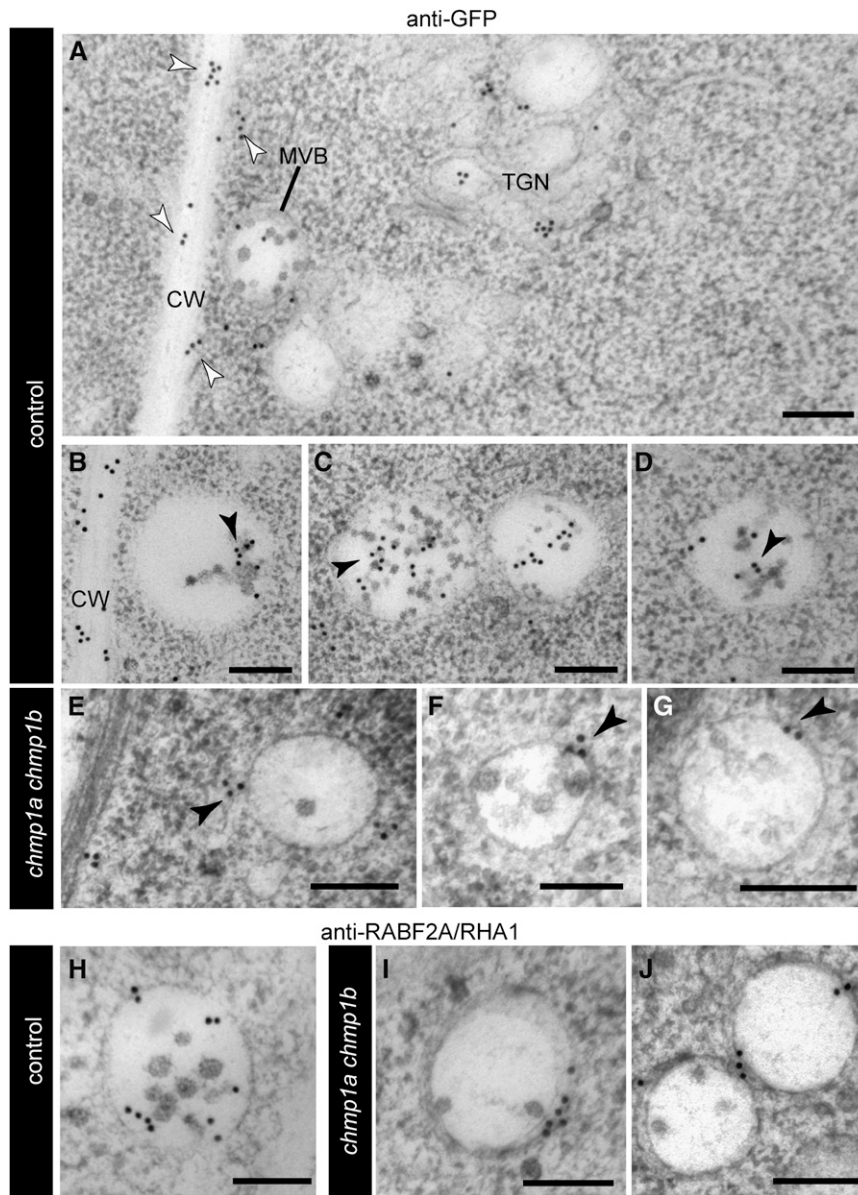
Figure 8. Immunogold Detection of PIN1-GFP and the Endosomal Marker RHA1/RabF2A in Control and Mutant MVBs.

(A) to **(G)** Immunolabeling of GFP in high-pressure frozen/freeze-substituted WT-looking (control) and *chmp1a chmp1b* mutant embryos expressing PIN1-GFP. CW, cell wall; TGN, *trans* Golgi network.
(A) Overview of a control embryo cell showing PIN1-GFP signal on the *trans* Golgi network, MVBs, and plasma membrane (white arrowheads).
(B) to **(D)** Detail of control MVBs with gold labeling on MVB lumenal vesicles (black arrowheads).
(E) to **(G)** Detail of *chmp1a chmp1b* mutant MVBs. Most of the gold labeling is on the MVB limiting membrane (black arrowheads) and not on MVB lumenal vesicles.
(H) to **(J)** Immunolabeling of RHA1/RABF2A on control **(H)** and *chmp1a chmp1b* mutant MVBs (**[I]** and **[J]**).
Bars = 200 nm.

Both PIN and AUX1 proteins have been shown to undergo constitutive recycling between the plasma membrane and endosomes (Geldner et al., 2001, 2003; Kleine-Vehn et al., 2006). PIN proteins seem to be first delivered to the plasma membrane in a nonpolar manner and acquire polarized localization by a mechanism that depends on endocytosis and endosomal recy-cling (Geldner et al., 2001; Jaillais et al., 2006; Dhonukshe et al., 2007, 2008; Kleine-Vehn et al., 2008b). The endosomal recycling of PIN1 depends on the Brefeldin A (BFA)–sensitive ARF-GEF GNOM, which has been hypothesized to localize to recycling endosomes (Geldner et al., 2003). The dynamic polar localization of PIN1 and PIN2 proteins depends on ARF-GEF–mediated

Table 2. Quantitative Analysis of MVB Structural Features in Embryos

	MVB Diameter (in nm)	Number of Lumenal Vesicles/Section	Percentage of Lumenal Vesicles Attached to MVB Membrane	Diameter of Lumenal Vesicles (in nm)
chmp1a chmp1b	276.2 ($\pm$65.6) * $n = 64$	1.0 * ($\pm$1.2)	53% *	35.6 ($\pm$7.3) $n = 71$
Control	346.2 ($\pm$57) * $n = 40$	5.6 * ($\pm$3.5)	10.7% *	35.0 ($\pm$7.5) $n = 182$

Only those endosomes labeled with the anti-RABF2A/RHA1 antibody were used for this analysis. Asterisks indicate that the difference between control and double mutant is significant at $P < 0.01$

transcytosis (the vesicular transport of macromolecules from one side of a cell to the other). Tissue-specific PIN1 and PIN2 basal localization seems to be GNOM dependent (Kleine-Vehn et al., 2008b). BFA treatment induces a basal-to-apical localization shift of PIN1 in the stele and PIN2 in cortex cells of wild-type plants but not in those plants expressing the engineered BFA-resistant GNOM[M696L] version (Kleine-Vehn et al., 2008b). The polarized localization of PIN proteins is also regulated by phosphorylation/dephosphorylation via the PINOID kinase and the PP2A phosphatase and by plasma membrane sterol composition (Friml et al., 2004; Michniewicz et al., 2007; Men et al., 2008). In addition, it has recently been shown that PGP19 (P-glycoprotein 19) stabilizes PIN1 localization at the plasma membrane (Titapiwatanakun et al., 2008).

The constitutive recycling of AUX1 does not depend on GNOM (Kleine-Vehn et al., 2006). Moreover, the limonoid-related chemical called endosidin 1 seems to affect the endosomal recycling of PIN2 and AUX1 but not of PIN1 (Robert et al., 2008). Interestingly, our results suggest that although PIN1, PIN2, and AUX1 do not entirely share the same endosomal recycling mechanisms, they are all MVB cargo proteins, sorted by the ESCRT machinery for vacuolar degradation.

Although we have not determined how these proteins are recognized by the ESCRT complexes, other studies have shown that at least one member of the PIN family, PIN2, becomes ubiquitinated (Abas et al., 2006). Ubiquitination of membrane proteins may also act as an MVB sorting signal in plants, as has been demonstrated in animals and yeast (Hicke and Dunn, 2003).

CHMP1 Is Necessary for Embryo Development

Although it is reasonable to think that the developmental alterations seen in chmp1a chmp1b mutant embryos are due to the missorting of numerous plasma membrane proteins, at least part of the embryo defects seem to be related to abnormal auxin accumulation patterns, as indicated by the expression of the DR5rev$_{pro}$:GFP reporter. In fact, many of the phenotypic alterations seen in the chmp1a chmp1b mutant, such as reduced polar differentiation and multiple rudimentary cotyledons, are commonly related to defects in auxin transport or auxin response (Vieten et al., 2007).

The mislocalization of PIN1, PIN2, and AUX1 in chmp1a chmp1b mutant embryos suggests that the abnormal DR5rev$_{pro}$:GFP

expression patterns in the mutant embryos may be due to altered cellular distribution of auxin transporters. Defects in the *Arabidopsis* Rab5 GTPase homolog ARA7/RabF2B, which also localizes to MVBs (Ueda et al., 2004; Haas et al., 2007), lead to loss in PIN polarization (Dhonukshe et al., 2008). Although expression of a dominant-negative form of the Rab GTPase ARA7/RabF2B does not affect the secretion of PIN1-GFP and PIN2-GFP to the plasma membrane, these proteins never acquire polarized distribution. Defects in the function of this Rab5 GTPase seem to compromise endocytosis (Dhonukshe et al., 2008) and, very likely, late endosomal functions as well.

In the chmp1a chmp1b mutant, PIN1 and PIN2 show only partially polarized localization (Figures 6H, 6I, 9M, and 9N). However, in contrast with the lines defective in Rab5 GTPase activity, the chmp1a chmp1b mutant is able to normally internalize the FM4-64 dye by endocytosis (Figures 9H and 9I). Although we have not established the mechanism by which the CHMP1 proteins affect polarized localization of PIN1 and PIN2, it is likely that defective MVB sorting and vacuolar degradation of membrane proteins cause a more general defect in other endosomal functions and/or in the endomembrane system as a whole. These defects in turn may affect the internalization and recycling rates of plasma membrane proteins.

Similar to what has been reported for the dominant-negative Rab5 lines (Dhonukshe et al., 2008), we have observed an enhanced DR5rev$_{pro}$:GFP signal in the cotyledons of chmp1a chmp1b mutant embryos (Figure 5). In addition, we have observed a strong GFP signal in procambial strands of mutant embryos. This could be interpreted as being the result of a reduced polar auxin transport from cotyledons to the root pole due to the missorting of auxin carriers. Deficient basipetal auxin transport could lead to the establishment of ectopic auxin maxima in the apical embryo region and to the formation of multiple, rudimentary cotyledons.

It is important to note that the partial missorting of PIN1, PIN2, and AUX1 cannot completely account for the altered auxin accumulation patterns and general developmental defects seen in the chmp1a chmp1b embryos. However, it is reasonable to think that many other auxin carriers are also affected by the chmp1a chmp1b double mutation. In fact, the combination of pin1, pin3, pin4, and pin7 mutations causes severe developmental defects that result in the formation of ball-shaped embryos (Friml et al., 2003) that closely resemble some of the most extreme chmp1a chmp1b embryo phenotypes.
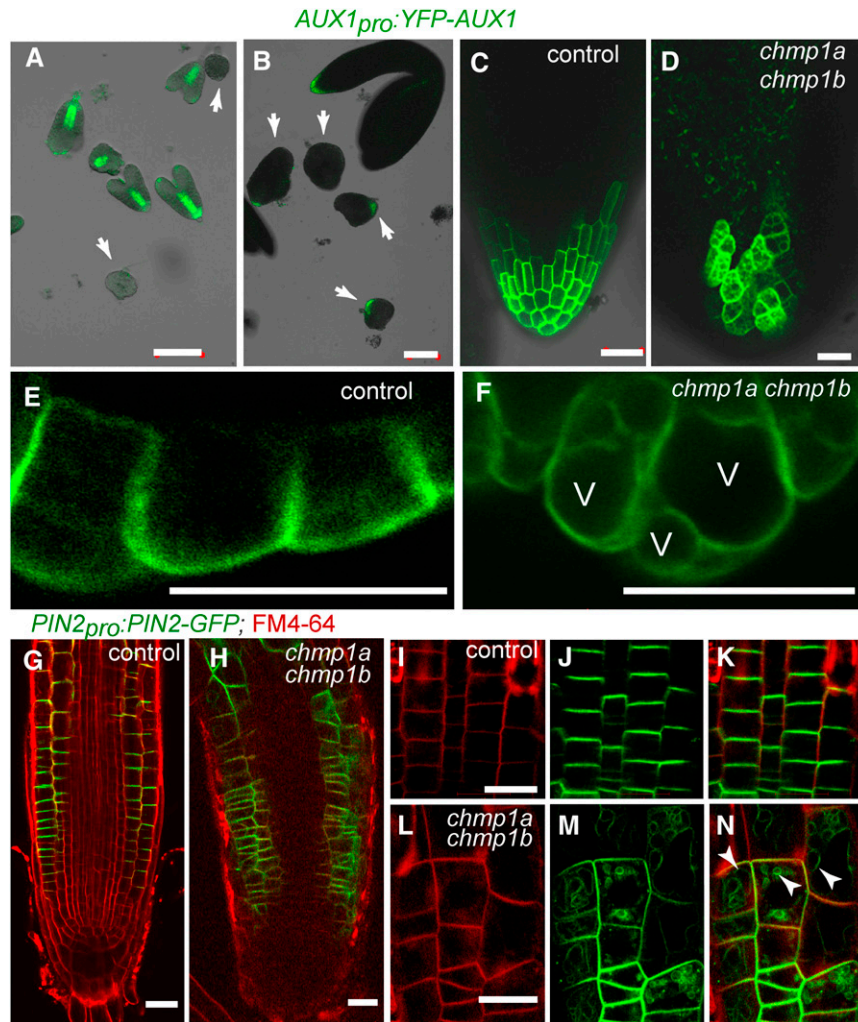
Figure 9. Expression Pattern and Subcellular Localization of AUX1-YFP and PIN2-GFP in Control and *chmp1a chmp1b* Mutant Embryos.

(A) and **(B)** Superimposed transmission and confocal images of control and *chmp1a chmp1b* mutant embryos expressing $AUX1_{pro}$:AUX1-YFP.

(A) Control embryos at the early torpedo stage expressed AUX1-YFP at the procambial strand and root pole, whereas the *chmp1a chmp1b* mutant embryos (arrows) do not express detectable levels of AUX1-GFP.

(B) Mature control and *chmp1a chmp1b* mutant embryos expressing AUX1-YFP at the root pole.

(C) and **(D)** Detail of control and *chmp1a chmp1b* mutant roots expressing AUX1-YFP.

(E) and **(F)** Control and *chmp1a chmp1b* embryo cells expressing AUX1-YFP at the root pole. Note the AUX1-YFP signal from the vacuolar membrane in mutant cells. V, vacuole.

(G) to **(N)** Expression of PIN2-GFP in epidermal and cortical cells in roots of control and *chmp1a chmp1b* mutant seedlings stained with FM4-64.

(I) to **(K)** Polarized localization of PIN2-GFP in the plasma membrane of epidermal cells in control roots.

(L) to **(N)** Localization of PIN2-GFP in *chmp1a chmp1b* root epidermal cells. Note the partial loss of polarized localization and the strong PIN2-GFP signal from vacuolar membranes (arrowheads).

Bars = 100 μm in **(A)** and **(B)** and 20 μm in **(C)** to **(N)**.

How General Is the Function of CHMP1 in the Sorting of Plasma Membrane Proteins?

The few *chmp1a chmp1b* mutant seeds that are able to germinate produce seedlings with additional defects, such as disorganized shoot and root apical meristems, rudimentary true leaves, clustered stomata, and enlarged epidermal root cells. It should be pointed out that many other membrane proteins, including plasma membrane transporters, channels, and receptors, are likely to be plant MVB cargo as well and therefore could also be mislocalized in the *chmp1a chmp1b* mutant. Although most mutant phenotypic defects described in this article, such as loss of polarity and impaired transition to embryo bilateral symmetry or altered leaf vein patterning, can be linked to auxin transport deficiencies, it is reasonable to think that many of the additional mutant defects might be due to alterations in the
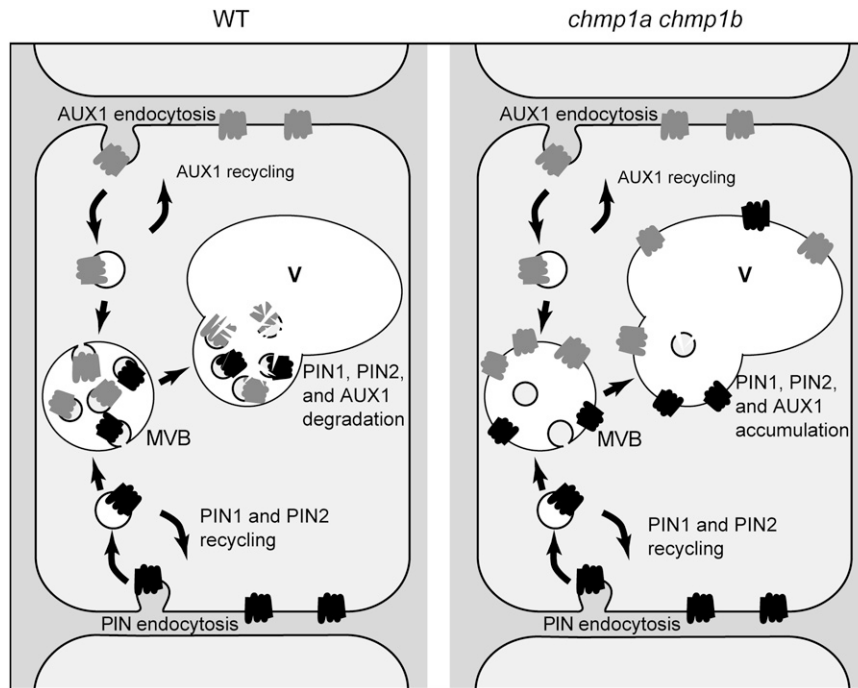
Figure 10. Model of CHMP1 Function in ESCRT-Mediated Sorting of Auxin Carriers.

AUX1, PIN1, and PIN2 cycle between endosomes and the plasma membrane by distinct mechanisms (Geldner et al., 2003; Kleine-Vehn et al., 2006; Robert et al., 2008). CHMP1 and ESCRT proteins mediate the degradation of PIN1, PIN2, and AUX1 in the vacuolar lumen in wild-type cells by sorting these proteins into MVB lumenal vesicles. In *chmp1a chmp1b* mutant cells, the sorting of PIN1, PIN2, and AUX1 and the formation of lumenal vesicles is compromised. As a result of MVB sorting defects, PIN1, PIN2, and AUX1 remain in the MVB limiting membrane and accumulate in the vacuolar membrane upon MVB vacuole fusion.

localization and degradation rate of multiple membrane proteins. This may be particularly evident in the stomata phenotype found in the *chmp1a chmp1b* double mutant. Stomata patterning involves leucine-rich repeat-containing receptor-like proteins. For example, TWO MANY MOUTH (TMM), ERECTA (ER), and ERECTA-like (ERL) are plasma membrane receptors that are required during stomata development for correct spacing (Nadeau and Sack, 2002; Shpak et al., 2005). Disruption of TMM or a combination of ER, ERL1, and ERL2 causes the formation of stomata clusters that are highly similar to those found in the *chmp1a chmp1b* double mutant (Yang and Sack, 1995).

In the case of activated membrane receptors, defective MVB sorting into lumenal vesicles may lead to the lack of receptor downregulation and constitutive signaling. In fact, the *sal1* mutant in maize, which showed reduced expression of the maize *CHMP1* homolog, *SAL1*, showed extra aleurone cell layers in the endosperm (Shen et al., 2003). Two plasma membrane proteins that are important positive regulators of aleurone differentiation, the receptor-like Ser/Thr kinase CRINKLY4 (CR4) and the calpain Cys protease DEFECTIVE KERNEL1 (DEK1), have been shown to colocalize with SAL1 on endosomes (Tian et al., 2007). If the maize knockdown *sal1* mutant is also deficient in MVB sorting as the *Arabidopsis chmp1a chmp1b* mutant, then CR4 and DEK1 may not be properly downregulated/degraded in the *sal1* mutant background, resulting in the differentiation of extra aleurone cells.

Although we only analyzed three proteins that are missorted in the absence of CHMP1, it is likely that many more are affected in a similar way. The *chmp1a chmp1b* mutant provides a tool to gain insights into plasma membrane protein degradation by ESCRT-mediated sorting.

METHODS

Plant Material and Conditions

The following seed stocks were obtained from the ABRC at Ohio State University: CS60000 (Col-0), SALK_135944 (*chmp1b-1*), SAIL_580CO3 (*chmp1a-1*), and CS9361 (*DR5rev:GFP*). *PIN1$_{pro}$:PIN1-GFP* (Heisler et al., 2005), *AUX1$_{pro}$:AUX1-YFP116* (Swarup et al., 2004), and *PIN2$_{pro}$:PIN2-GFP* (Laxmi et al., 2008) were kindly provided by E.M. Meyerowitz, M.J. Bennett, and R. Chen.

Arabidopsis thaliana seeds were planted on Jiffy Mix #901 (www. lgproducts.com) supplemented with Vermiculite (www.fertilome.com), stratified for 4 d at 4°C, and grown at 22 ± 3°C under a 16-h-light/8-h-dark cycle. For growing seedlings on agar-containing plates, *Arabidopsis* seeds were pretreated in 70% ethanol for 5 min, surface-sterilized in 50% bleach for 1 min, and washed with distillated water at least five times. Seeds were planted on 1% agar-containing 0.8× Murashige and Skoog salts, stratified, and grown as described above. Selection of transgenic seedlings was performed on agar plates supplemented with 20 μg/mL of hygromycin (PhytoTechnology Laboratories).

The wild-type background of the *chmp1a-1* and *chmp1b-1* alleles is Col-0. *chmp1a chmp1b* double mutants were isolated from plants

homozygous for *chmp1a-1* and heterozygous for *chmp1b-1*. The *chmp1b-1* insertion was detected by PCR genotyping with primers SALK135944f (5′-GGACATAATGTTAGGAAGCC-3′) and SALK-LBa1 (5′-TGGTTCACGTAGTGGGCCATCG-3′). The *chmp1a-1* insertion was detected with primers SAIL580-CO3f (5′-CATCGGACGGTGCTGAG-3′) and SAIL-LB (5′-GCCTTTTCAGAAATGGATAAATAGCC-3′). The corresponding wild-type primers are SALK135944r (5′-CATTGTAAAAACA-CACTC-3′) and SAIL580-CO3r (5′-CACGAAGGTTTTTTATATAAA-3′). Siliques and developing seeds from these plants were dissected, and calli formed from isolated embryos were genotyped by PCR. F3 lines derived from crosses between *chmp1a-1/chmp1a-1 chmp1b-1/CHMP1B* and either *PIN1_{pro}:PIN1-GFP*, *AUX1pro:AUX1-YFP116*, *PIN2_{pro}:PIN2-GFP*, or *DR5rev_{pro}:GFP* were genotyped to isolate plants heterozygous for *CHMP1B* and homozygous for *chmp1a-1* and the fluorescent protein markers. Controls in all cases were wild type–looking embryos dissected from the same siliques or seedlings from the mother plant.

To induce proliferation of calli, wild-type and *chmp1a chmp1b* mutant embryos were placed on agar plates containing 10 μM 2,4-D (Wei et al., 2006).

Complementation of the *chmp1a chmp1b* Double Mutant

For rescuing the *chmp1a chmp1b* mutant, a genomic fragment of CHMP1B was introduced by *Agrobacterium tumefaciens*–mediated transformation into *CHMP1A/chmp1a chmp1b/chmp1b plants*. The genomic region of *At1g17730* (*CHMP1B*) was PCR amplified with Phusion polymerase (New England Biolabs) using primers PCS015-Sal2 (5′-TAG-GATCCACTCCACTCTAAAGACG-3′) and PCS016-Sal2 (5′-GTTTGAC-GCTTGTTGC-3′). The resulting 3.2-kb band was column purified and ligated blunt into the *Ecl136II* site of binary vector *pCAMBIA1300*. DNA was transformed into JM109 competent *Escherichia coli*, and the resulting clone B008 was transformed into *A. tumefaciens* strain GV3101 containing *pMP90*. Binary vectors were introduced into *Arabidopsis* using the floral dip method (Clough and Bent, 1998). T1 plants were genotyped to identify viable homozygous double mutants.

Expression Analysis

RNA was extracted from plant tissue using TriPure Reagent (Roche Applied Science) from plants that were confirmed as being homozygous for the mutant alleles via PCR genotyping. RT-PCR was performed using the AccessQuick RT-PCR System (Promega) with the following primers: CHMP1A F 5′-ATA<u>ACGCGT</u>ATG GGTAACACAGATAAGC-3′, CHMP1A R 5′-CACGAAGG<u>TTTTTTATATAAAG</u>-3′; CHMP1B F 5′-TTTCCCCAA-ATTCGAAAGAAC-3′, CHMP1B R 5′-CATTGTAAAAACACACTC-3′; and actin F 5′-GACTCAAATCATGTTTGAGACC-3′, actin R 5′-CATTTTCTGT-GAACGATTCCT-3′. The underlined region corresponds to a restriction site and is not complementary to the CHMP1A sequence. PCR amplification products were separated in 1% agarose gels and visualized with ethidium bromide.

Confocal Imaging of Fluorescent Proteins and FM4-64

Embryos were dissected from developing seeds ~5 to 15 d after pollination to obtain globular to mature embryo stages. Embryos were rinsed in water, incubated for 30 s in 4 μM FM4-64 (Invitrogen), and rinsed prior to observation. Imaging was performed with a Zeiss LSM 510 META confocal laser scanning microscope. To visualize GFP or YFP/FM4-64, the following settings were used. GFP/FM4-64: GFP excited with 488 nm and emission collected with BP 500-530 IR; FM4-64 excited with 543 nm and emission collected with BP 565-616 IR (multitrack mode). YFP/FM4-64: YFP excited with 488 nm and emission collected with BP 500-550 IR; FM4-64 excited with 543 nm intensity and emission collected with BP

565-616 IR (multitrack mode). Alternatively, the Meta detector was used to visualize FM4-64: Excitation with the 514- or 543-nm laser line and emission collected between 602 and 644 nm. GFP or YFP/bright-field images were acquired using the transmission detector of the microscope in combination with the above settings.

For structural analysis of roots, 4-week-old seedlings were stained with propidium iodide for 5 min, rinsed in distilled water, and imaged. For excitation of propidium iodide, the 543-nm excitation line of the HeNe laser was used and emission was collected with a 560-nm long-pass filter.

Images were edited using the LSM image browser (http://www.zeiss.com/lsm) and Adobe Photoshop CS3.

Electron Microscopy and Immunolabeling

Arabidopsis embryos were high-pressure frozen/freeze-substituted for electron microscopy analysis as described previously (Otegui et al., 2006).

For immunolabeling, high-pressure frozen samples were substituted in 0.2% uranyl acetate (Electron Microscopy Sciences) plus 0.2% glutaraldehyde (Electron Microscopy Sciences) in acetone at −80°C for 72 h and warmed to −50°C for 24 h. After several acetone rinses, these samples were infiltrated with Lowicryl HM20 (Electron Microscopy Sciences) for 72 h and polymerized at −50°C under UV light for 48 h. Sections were mounted on formvar-coated nickel grids and blocked for 20 min with a 5% (w/v) solution of nonfat milk in PBS containing 0.1% Tween 20. The sections were incubated in the primary polyclonal antibodies against RABF2A/RHA1 (Haas et al., 2007), anti-GFP (Follet-Gueye et al., 2003), or anti-2S albumins (Scarafoni et al., 2001) (1:10 in PBS-Tween 20) for 1 h, rinsed in PBS containing 0.5% Tween 20, and then transferred to the secondary antibody (anti-rabbit IgG 1:10) conjugated to 15-nm gold particles for 1 h. Controls lacked the primary antibodies.

In Vitro Interaction Assay

CHMP1A was amplified from cDNA clone U16228 (ABRC) using primers 5′-CACC<u>GAATTC</u>ATGGGTAACACAGATAAGC-3′ and 5′-CCA-A<u>CTCGAG</u>TTATCCTCTGGCTTTAAG-3′ (*Eco*RI and *Xho*I restriction sites are underlined) and cloned into the pGEX vector. For the HIS fusion, primers 5′-CACC<u>GAATTC</u>ATGGGTAACACAGATAAGC-3′ and 5′-AAA<u>GTCG-AC</u>TTATCCTCTGGCTTTAAG-3′ (that contain *Eco*RI and *Sal*I restriction sites, underlined) were used to amplify CHMP1A, and the products were ligated into the pET vector.

LIP5 (At4g26750) was amplified from LIP5 cDNA clone U13054 (ABRC) using primers 5′-AAA<u>GAATTC</u>ATGTCGAACCCAAACG-3′ and 5′-AAA<u>GTCGAC</u>TCAGTGACCGGCACC-3′ and cloned into the pGEX vector using the *Eco*RI and *Sal*I sites to create the N-terminal GST fusion protein.

For the expression of GST alone, the pGEX vector (Amersham) was used. The cloning and protein expression of 6xHis-SKD1 was described by Haas et al. (2007). All vectors were sequenced and transformed into *E. coli* BL21 for protein expression. GST fusion proteins were purified using glutathione-agarose beads (Sigma-Aldrich), and 6XHis-fusion proteins were purified using NiNTA agarose beads (Qiagen). For the in vitro interaction pull-down experiments, equivalent amounts of purified GST-CHMP1A or GST-LIP5 proteins bound to glutathione agarose beads and 6xHis-SKD1 or 6xHis-CHMP1A were incubated overnight at 4°C in 20 mM HEPES, pH 7.4, 300 mM NaCl, 5 mM MgCl₂, 10% glycerol, and 0.02% Nonidet P-40 (input). The glutathione agarose beads were then rinsed three times with the same buffer described above except that 0.2% of Nonidet P-40 was used (output). Both samples were denatured using Laemmli buffer, separated by SDS-PAGE, and transferred onto a nitrocellulose membrane. The proteins were detected using the

anti-6xHis antibody (Sigma-Aldrich) and the anti-GST antibody (kindly donated by Sebastian Bednarek, University of Wisconsin–Madison).

Protein Gel Blot Analysis

Total protein extracts were obtained by grinding ~115 mg of wild-type and *chmp1a chmp1b* embryos in protein extraction buffer (20 mM Tris-HCl, pH 7.5, 5 mM EDTA, and 2 μM β-mercaptoethanol) with protease inhibitors (Roche). The extracts were spun for 10 min at 4°C, and the supernatant was loaded on SDS-PAGE gel with loading buffer. SDS-PAGE and blotting were performed in Bio-Rad Mini Protean 3 and Bio-Rad Trans according to manufacturer's manual. The nitrocellulose membrane was incubated in a 1:1000 dilution of anti-SAL1 (Tian et al., 2007), and 1:1000 anti-Rubisco (Martínez et al., 2008) antibodies in PBS-0.5% Tween 20 were used in a 1:1000 dilution. The immune detection signals were visualized with the ECL+Plus system (GE Healthcare).

Phylogenetic Analysis

The CHMP1-related protein sequences where obtained from GeneBank and aligned using ClustalW (Larkin et al., 2007). Maximum likelihood–based inference and bootstrap analyses to estimate clade support were performed using the RAxML 7.0.4 (Randomized Axelerated Maximum Likelihood) software (Stamatakis et al., 2008). The resulting best tree was displayed and rooted using TreeView 1.6.6 (http://taxonomy.zoology.gla.ac.uk/rod/rod/html). *Trypanosoma* and *Leishmania* were chosen as out-group.

Accession Numbers

Sequence data from this article can be found in the Arabidopsis Genome Initiative or GenBank/EMBL databases under the following accession numbers: *CHMP1A* (At1g73030), *CHMP1B* (At1g17730), At2g27600 (SKD1), At4g26750 (LIP5), *Anopheles gambiae* (mosquito) CHMP1 (XP_316550), *Arabidopsis* CHMP1A (At1g17730), *Arabidopsis* CHMP1B (At1g73030), *Candida glabrata* DID2 (XP_448910), *Caenorhabditis elegans* CHMP1 (NP_490974), *Chlamydomonas reinhardtii* CHMP1 (EDP04347), *Danio rerio* (zebrafish) CHMP1A (NP_956857), *D. rerio* CHMP1B (NP_956308), *Drosophila melanogaster* (fruitfly) CHMP1 (NP_649051), *Gallus gallus* (chicken) CHMP1A (NP_001020611 XP_414202), *G. gallus* CHMP1B (NP_001006428 XP_420145), *Homo sapiens* (human) CHMP1A (NP_002759), *H. sapiens* CHMP1B (AAG01449), *Hordeum vulgare* (barley) (ABW81400), *Laccaria bicolor* DID2 (XP_001876605), *Leishmania major* CHMP1(XP_843546), *Nicotiana benthamiana* CHMP1 (AAO59435), Oryza sativa (rice) CHMP1 (Os06g0643300), *Physcomitrella patens* CHMP1C (EDQ70932), *Physcomitrella patens* CHMP1D (EDQ75198), *P. patens* CHMP1B (EDQ50729), *P. patens* CHMP1A DID2 (XP_001384837), *Pichia stipitis* DID2 (XP_001384837), *Saccharomyces cerevisiae* (budding yeast) DID2 (NP_012961), *Trypanosoma brucei* CHMP1 (XP_827323), *Schyzosaccharomyces pombe* (fission yeast) DID2 (NP_596562), *Strongylocentrotus purpuratus* (purple sea urchin) CHMP1A(XP_780596), *S. purpuratus* CHMP1B(XP_001190962), *Ustilago maydis* (EAK86473), *Xenopus laevis* (African frog) CHMP1A (NP_001084706), *Xenopus* CHMP1B (Q7SZB5), and *Zea mays* (maize) SAL1 (NP_001105218).

Supplemental Data

The following materials are available in the online version of this article.

Supplemental Figure 1. Alignment of CHMP1 Protein Sequences.

Supplemental Figure 2. Phenotype of Wild-Type, *chmp1* Mutant, and Rescued *chmp1a chmp1b* Mutant Seedlings.

Supplemental Figure 3. Localization of PIN1-GFP in Control and Mutant Embryos after Dark Treatment.

Supplemental Figure 4. Control Labeling Using Anti-GFP Antibodies on Wild-Type Heart Stage Embryos.

Supplemental Figure 5. Immunolabeling of 2S Albumins in PSVs of Wild-Type and *chmp1a chmp1b* Mutant Embryos.

Supplemental Data Set 1. Sequences Used to Generate the Phylogeny in Figure 1A.

REFERENCES

Abas, L., Benjamins, R., Malenica, N., Paciorek, T., Wisniewska, J., Moulinier-Anzola, J.C., Sieberer, T., Friml, J., and Luschnig, C. (2006). Intracellular trafficking and proteolysis of the *Arabidopsis* auxin-efflux facilitator PIN2 are involved in root gravitropism. Nat. Cell Biol. **8:** 249–256.

Azmi, I., Davies, B., Dimaano, C., Payne, J., Eckert, D., Babst, M., and Katzmann, D.J. (2006). Recycling of ESCRTs by the AAA-ATPase Vps4 is regulated by a conserved VSL region in Vta1. J. Cell Biol. **172:** 705–717.

Azmi, I.F., Davies, B.A., Xiao, J., Babst, M., Xu, Z., and Katzmann, D.J. (2008). ESCRT-III family members stimulate Vps4 ATPase activity directly or via Vta1. Dev. Cell **14:** 50–61.

Babst, M. (2005). A protein's dinal ESCRT. Traffic **6:** 2–9.

Babst, M., Sato, T.K., Banta, L.M., and Emr, S.D. (1997). Endosomal transport function in yeast requires a novel AAA-type ATPase, Vps4p. EMBO J. **16:** 1820–1831.

Babst, M., Wendland, B., Estepa, E.J., and Emr, S.D. (1998). The Vps4p AAA ATPase regulates membrane association of a Vps protein complex required for normal endosome function. EMBO J. **17:** 2982–2993.

Bowers, K., Lottridge, J., Helliwell, S.B., Goldthwaite, L.M., Luzio, J.P., and Stevens, T.H. (2004). Protein-protein interactions of ESCRT xomplexes in the yeast *Saccharomyces cerevisiae.* Traffic **5:** 194–210.

Clough, S.J., and Bent, A.F. (1998). Floral dip: A simplified method for *Agrobacterium*-mediated transformation of *Arabidopsis thaliana.* Plant J. **16:** 735–743.

Dhonukshe, P., Aniento, F., Hwang, I., Robinson, D.G., Mravec, J., Stierhof, Y.-D., and Friml, J. (2007). Clathrin-mediated constitutive endocytosis of PIN auxin efflux carriers in *Arabidopsis*. Curr. Biol. **17:** 520–527.

Dhonukshe, P., et al. (2008). Generation of cell polarity in plants links endocytosis, auxin distribution and cell fate decisions. Nature **456:** 962–966.

Dimaano, C., Jones, C.B., Hanono, A., Curtiss, M., and Babst, M. (2008). Ist1 regulates Vps4 localization and assembly. Mol. Biol. Cell **19:** 465–474.

Follet-Gueye, M.-L., Pagny, S., Faye, L., Gomord, V., and Driouich, A. (2003). An improved chemical fixation method suitable for immunogold localization of green fluorescent protein in the Golgi apparatus of tobacco Bright Yellow (BY-2) cells. J. Histochem. Cytochem. **51:** 931–940.

Friml, J., Vieten, A., Sauer, M., Weijers, D., Schwarz, H., Hamann, T., Offringa, R., and Jurgens, G. (2003). Efflux-dependent auxin gradients establish the apical-basal axis of *Arabidopsis*. Nature **426:** 147–153.

Friml, J., et al. (2004). A PINOID-dependent binary switch in apical-basal PIN polar targeting directs auxin efflux. Science **306:** 862–865.

Geldner, N., Anders, N., Wolters, H., Keicher, J., Kornberger, W., Muller, P., Delbarre, A., Ueda, T., Nakano, A., and Jurgens, G. (2003). The *Arabidopsis* GNOM ARF-GEF mediates endosomal recycling, auxin transport, and auxin-dependent plant growth. Cell **112:** 219–230.

Geldner, N., Friml, J., Stierhof, Y., Jurgens, G., and Palme, K. (2001). Auxin transport inhibitors block PIN1 cycling and vesicle trafficking. Nature **413:** 425–428.

Gruenberg, J., and Stenmark, H. (2004). The biogenesis of multivesicular endosomes. Nat. Rev. Mol. Cell Biol. **5:** 317–323.

Haas, T.J., Sliwinski, M.K., Martínez, D.E., Preuss, M., Ebine, K., Ueda, T., Nielsen, E., Odorizzi, G., and Otegui, M.S. (2007). The *Arabidopsis* AAA ATPase SKD1 is involved in multivesicular endosome function and interacts with its positive regulator LYST-INTERACTING PROTEIN5. Plant Cell **19:** 1295–1312.

Heisler, M.G., Ohno, C., Das, P., Sieber, P., Reddy, G.V., Long, J.A., and Meyerowitz, E.M. (2005). Patterns of auxin transport and gene expression during primordium development revealed by live imaging of the *Arabidopsis* inflorescence meristem. Curr. Biol. **15:** 1899–1911.

Hicke, L., and Dunn, R. (2003). Regulation of membrane protein transport by ubiquitin and ubiquitin-binding proteins. Annu. Rev. Cell Dev. Biol. **19:** 141–172.

Hurley, J.H., and Emr, S.D. (2006). The ESCRT complexes: Structure and mechanism of a membrane-trafficking network. Annu. Rev. Biophys. Biomol. Struct. **35:** 277–298.

Jaillais, Y., Fobis-Loisy, I., Miege, C., Rollin, C., and Gaude, T. (2006). AtSNX1 defines an endosome for auxin-carrier trafficking in *Arabidopsis*. Nature **443:** 106–109.

Jaillais, Y., Santambrogio, M., Rozier, F., Fobis-Loisy, I., Miege, C., and Gaude, T. (2007). The retromer protein VPS29 links cell polarity and organ initiation in plants. Cell **130:** 1057–1070.

Jou, Y., Chiang, C.-P., Jauh, G.-Y., and Yen, H.E. (2006). Functional characterization of ice plant SKD1, an AAA-Type ATPase associated with the endoplasmic reticulum-Golgi network, and its role in adaptation to salt stress. Plant Physiol. **141:** 135–146.

Katzmann, D.J., Babst, M., and Emr, S.D. (2001). Ubiquitin-dependent sorting into the multivesicular body pathway requires the function of a conserved endosomal protein sorting complex, ESCRT-I. Cell **106:** 145–155.

Katzmann, D.J., Odorizzi, G., and Emr, S.D. (2002). Receptor downregulation and multivesicular-body sorting. Nat. Rev. Mol. Cell Biol. **3:** 893–905.

Katzmann, D.J., Stefan, C.J., Babst, M., and Emr, S.D. (2003). Vps27 recruits ESCRT machinery to endosomes during MVB sorting. J. Cell Biol. **162:** 413–423.

Kleine-Vehn, J., Dhonukshe, P., Sauer, M., Brewer, P.B., Wisniewska, J., Paciorek, T., Benková, E., and Friml, J. (2008b). ARF GEF-dependent transcytosis and polar delivery of PIN auxin carriers in *Arabidopsis*. Curr. Biol. **18:** 526–531.

Kleine-Vehn, J., Dhonukshe, P., Swarup, R., Bennett, M., and Friml, J. (2006). Subcellular trafficking of the *Arabidopsis* auxin influx carrier AUX1 uses a novel pathway distinct from PIN1. Plant Cell **18:** 3171–3181.

Kleine-Vehn, J., Leitner, J., Zwiewka, M., Sauer, M., Abas, L., Luschnig, C., and Friml, J. (2008a). Differential degradation of PIN2 auxin efflux carrier by retromer-dependent vacuolar targeting. Proc. Natl. Acad. Sci. USA **105:** 17812–17817.

Larkin, M.A., et al. (2007). Clustal W and Clustal X version 2.0. Bioinformatics **23:** 2947–2948.

Laxmi, A., Pan, J., Morsy, M., and Chen, R. (2008). Light plays an essential role in intracellular distribution of auxin efflux carrier PIN2 in *Arabidopsis thaliana*. PLoS One **3:** e1510.

Leung, K.F., Dacks, J.B., and Field, M.C. (2008). Evolution of the multivesicular body ESCRT machinery; retention across the eukaryotic lineage. Traffic **9:** 1698–1716.

Li, J., Belogortseva, N., Porter, D., and Park, M. (2008). Chmp1A functions as a novel tumor suppressor gene in human embryonic kidney and ductal pancreatic tumor cells. Cell Cycle **7:** 2886–2893.

Lin, Y., Kimpler, L.A., Naismith, T.V., Lauer, J.M., and Hanson, P.I. (2005). Interaction of the mammalian endosomal sorting complex required for transport (ESCRT) III protein hSnf7-1 with itself, membranes, and the AAA+ ATPase SKD1. J. Biol. Chem. **280:** 12799–12809.

Lottridge, J.M., Flannery, A.R., Vincelli, J.L., and Stevens, T.H. (2006). Vta1p and Vps46p regulate the membrane association and ATPase activity of Vps4p at the yeast multivesicular body. Proc. Natl. Acad. Sci. USA **103:** 6202–6207.

Lupas, A., Van Dyke, M., and Stock, J. (1991). Predicting coiled coils from protein sequences. Science **252:** 1162–1164.

Martínez, D.E., Costa, M.L., Otegui, M.S., and Guiamet, J.J. (2008). Senescence-associated vacuoles of tobacco leaves are involved in the degradation of chloroplast proteins. Plant J. **56:** 192–206.

Men, S., Boutte, Y., Ikeda, Y., Li, X., Palme, K., Stierhof, Y.D., Hartmann, M.A., Moritz, T., and Grebe, M. (2008). Sterol-dependent endocytosis mediates post-cytokinetic acquisition of PIN2 auxin efflux carrier polarity. Nat. Cell Biol. **10:** 237–244.

Michniewicz, M., et al. (2007). Antagonistic regulation of PIN phosphorylation by PP2A and PINOID directs auxin flux. Cell **130:** 1044–1056.

Muday, G.K., Peer, W.A., and Murphy, A.S. (2003). Vesicular cycling mechanisms that control auxin transport polarity. Trends Plant Sci. **8:** 301–304.

Mullen, R.T., McCartney, A.W., Flynn, C.R., and Smith, G.S.T. (2006). Peroxisome biogenesis and the formation of multivesicular peroxisomes during tombusvirus infection: a role for ESCRT? Can. J. Bot. **84:** 551–564.

Muller, J., Mettbach, U., Menzel, D., and Samaj, J. (2007). Molecular dissection of endosomal compartments in plants. Plant Physiol. **145:** 293–304.

Nadeau, J.A., and Sack, F.D. (2002). Control of stomatal distribution on the *Arabidopsis* leaf surface. Science **296:** 1697–1700.

Nickerson, D.P., Russell, M.R., and Odorizzi, G. (2007). A concentric circle model of multivesicular body cargo sorting. EMBO Rep. **8:** 644–650.

Nickerson, D.P., West, M., and Odorizzi, G. (2006). Did2 coordinates Vps4-mediated dissociation of ESCRT-III from endosomes. J. Cell Biol. **175:** 715–720.

Obita, T., Saksena, S., Ghazi-Tabatabai, S., Gill, D.J., Perisic, O., Emr, S.D., and Williams, R.L. (2007). Structural basis for selective

recognition of ESCRT-III by the AAA ATPase Vps4. Nature **449:** 735–739.

Otegui, M.S., Herder, R., Schulze, J.M., Jung, R., and Staehelin, L.A. (2006). The proteolytic processing of seed storage proteins in *Arabidopsis* embryo cells starts in the multivesicular bodies. Plant Cell **18:** 2567–2581.

Ottenschläger, I., Wolff, P., Wolverton, C., Bhalerao, R.P., Sandberg, G., Ishikawa, H., Evans, M., and Palme, K. (2003). Gravity-regulated differential auxin transport from columella to lateral root cap cells. Proc. Natl. Acad. Sci. USA **100:** 2987–2991.

Piper, R.C., and Katzmann, D.J. (2007). Biogenesis and function of multivesicular bodies. Annu. Rev. Cell Dev. Biol. **23:** 519–547.

Reggiori, F., and Pelham, H.R. (2001). Sorting of proteins into multivesicular bodies: ubiquitin-dependent and -independent targeting. EMBO J. **20:** 5176–5186.

Richter, C., West, M., and Odorizzi, G. (2007). Dual mechanisms specify Doa4-mediated deubiquitination at multivesicular bodies. EMBO J. **26:** 2454–2464.

Robert, S., Chary, S.N., Drakakaki, G., Li, S., Yang, Z., Raikhel, N.V., and Hicks, G.R. (2008). Endosidin1 defines a compartment involved in endocytosis of the brassinosteroid receptor BRI1 and the auxin transporters PIN2 and AUX1. Proc. Natl. Acad. Sci. USA **105:** 8464–8469.

Robinson, D.G., Jiang, L., and Schumacher, K. (2008). The endosomal system of plants: charting new and familiar territories. Plant Physiol. **147:** 1482–1492.

Rue, S.M., Mattei, S., Saksena, S., and Emr, S.D. (2008). Novel ist1-did2 complex functions at a late step in multivesicular body sorting. Mol. Biol. Cell **19:** 475–484.

Russell, M.R.G., Nickerson, D.P., and Odorizzi, G. (2006). Molecular mechanisms of late endosome morphology, identity and sorting. Curr. Opin. Cell Biol. **18:** 422–428.

Scarafoni, A., Carzaniga, R., Harris, N., and Croy, R. (2001). Manipulation of the napin primary structure alters its packaging and deposition in transgenic tobacco (*Nicotiana tabacum* L.) seeds. Plant Mol. Biol. **46:** 727–739.

Scott, A., Chung, H., Gonciarz-Swiatek, M., Hill, G., Whitby, F., Gaspar, J., Holton, J., Viswanathan, R., Ghaffarian, S., Hill, C., and Sundquist, W. (2005b). Structural and mechanistic studies of VPS4 proteins. EMBO J. **24:** 3658–3669.

Scott, A., Gaspar, J., Stuchell-Brereton, M.D., Alam, S.L., Skalicky, J.J., and Sundquist, W.I. (2005a). Structure and ESCRT-III protein interactions of the MIT domain of human VPS4A. Proc. Natl. Acad. Sci. USA **102:** 13813–13818.

Shen, B., Li, C., Min, Z., Meeley, R.B., Tarczynski, M.C., and Olsen, O.-A. (2003). Sal1 determines the number of aleurone cell layers in maize endosperm and encodes a class E vacuolar sorting protein. Proc. Natl. Acad. Sci. USA **100:** 6552–6557.

Shpak, E.D., McAbee, J.M., Pillitteri, L.J., and Torii, K.U. (2005). Stomatal patterning and differentiation by synergistic interactions of receptor kinases. Science **309:** 290–293.

Sieburth, L.E., Muday, G.K., King, E.J., Benton, G., Kim, S., Metcalf, K.E., Meyers, L., Seamen, E., and Van Norman, J.M. (2006). SCARFACE encodes an ARF-GAP that is required for normal auxin efflux and vein patterning in *Arabidopsis.* Plant Cell **18:** 1396–1411.

Spitzer, C., and Otegui, M.S. (2008). Endosomal functions in plants. Traffic **9:** 1589–1598.

Spitzer, C., Schellmann, S., Sabovljevic, A., Shahriari, M., Keshavaiah, C., Bechtold, N., Herzog, M., Muller, S., Hanisch, F.G., and Hulskamp, M. (2006). The Arabidopsis *elch* mutant reveals functions of an ESCRT component in cytokinesis. Development **133:** 4679–4689.

Stamatakis, A., Hoover, P., and Rougemont, J. (2008). A fast bootstrapping algorithm for the RAxML Web-servers. Syst. Biol. **57:** 758–771.

Stauffer, D.R., Howard, T.L., Nyun, T., and Hollenberg, S.M. (2001). CHMP1 is a novel nuclear matrix protein affecting chromatin structure and cell-cycle progression. J. Cell Sci. **114:** 2383–2393.

Steinmann, T., Geldner, N., Grebe, M., Mangold, S., Jackson, C.L., Paris, S., Gälweiler, L., Palme, K., and Jurgens, G. (1999). Coordinated polar localization of auxin efflux carrier PIN1 by GNOM ARF GEF. Science **286:** 316–318.

Stuchell-Brereton, M.D., Skalicky, J.J., Kieffer, C., Karren, M.A., Ghaffarian, S., and Sundquist, W.I. (2007). ESCRT-III recognition by VPS4 ATPases. Nature **449:** 740–744.

Swarup, R., et al. (2004). Structure-function analysis of the presumptive *Arabidopsis* auxin permease AUX1. Plant Cell **16:** 3069–3083.

Teis, D., Saksena, S., and Emr, S.D. (2008). Ordered assembly of the ESCRT-III complex on endosomes is required to sequester cargo during MVB formation. Dev. Cell **15:** 578–589.

Tian, Q., Olsen, L., Sun, B., Lid, S.E., Brown, R.C., Lemmon, B.E., Fosnes, K., Gruis, D., Opsahl-Sorteberg, H.-G., Otegui, M.S., and Olsen, O.-A. (2007). Subcellular localization and functional domain studies of DEFECTIVE KERNEL1 in maize and *Arabidopsis* suggest a model for aleurone cell fate specification involving CRINKLY4 and SUPERNUMERARY ALEURONE LAYER1. Plant Cell **19:** 3127–3145.

Titapiwatanakun, B., et al. (2008). ABCB19/PGP19 stabilises PIN1 in membrane microdomains in Arabidopsis. Plant J. **57:** 27–44.

Tsang, H.T., Connell, J.W., Brown, S.E., Thompson, A., Reid, E., and Sanderson, C.M. (2006). A systematic analysis of human CHMP protein interactions: Additional MIT domain-containing proteins bind to multiple components of the human ESCRT III complex. Genomics **88:** 333–346.

Ueda, T., Uemura, T., Sato, M.H., and Nakano, A. (2004). Functional differentiation of endosomes in *Arabidopsis* cells. Plant J. **40:** 783–789.

Vajjhala, P.R., Catchpoole, E., Nguyen, C.H., Kistler, C., and Munn, A.L. (2007). Vps4 regulates a subset of protein interactions at the multivesicular endosome. FEBS J. **274:** 1894–1907.

Vajjhala, P.R., Wong, J.S., To, H.-Y., and Munn, A.L. (2006). The β domain is required for Vps4p oligomerization into a functionally active ATPase. FEBS J. **273:** 2357–2373.

Vieten, A., Sauer, M., Brewer, P.B., and Friml, J. (2007). Molecular and cellular aspects of auxin-transport-mediated development. Trends Plant Sci. **12:** 160–168.

Wei, J., Li, X.-R., and Sun, M.X. (2006). Establishment of a simple and efficient system for somatic embryo induction via ovule culture in *Arabidopsis thaliana.* Plant Cell Rep. **25:** 1275–1280.

Winter, V., and Hauser, M.-T. (2006). Exploring the ESCRTing machinery in eukaryotes. Trends Plant Sci. **11:** 115–123.

Yang, D., Rismanchi, N., Renvoise, B., Lippincott-Schwartz, J., Blackstone, C., and Hurley, J.H. (2008). Structural basis for midbody targeting of spastin by the ESCRT-III protein CHMP1B. Nat. Struct. Mol. Biol. **15:** 1278–1286.

Yang, K.S., Jin, U.H., Kim, J., Song, K., Kim, S.J., Hwang, I, Lim, Y.P., and Pai, H.S. (2004). Molecular characterization of NbCHMP1 encoding a homolog of human CHMP1 in *Nicotiana benthamiana.* Mol. Cells **17:** 255–261.

Yang, M., and Sack, F.D. (1995). The *too many mouths* and *four lips* mutations affect stomatal production in *Arabidopsis.* Plant Cell **7:** 2227–2239.

Yeo, S.C., et al. (2003). Vps20p and Vta1p interact with Vps4p and function in multivesicular body sorting and endosomal transport in *Saccharomyces cerevisiae.* J. Cell Sci. **116:** 3957–3970.

Yoshimori, T., Yamagata, F., Yamamoto, A., Mizushima, N., Kabeya, Y., Nara, A., Miwako, I., Ohashi, M., Ohsumi, M., and Ohsumi, Y. (2000). The mouse SKD1, a homologue of yeast Vps4p, is required for normal endosomal trafficking and morphology in mammalian cells. Mol. Biol. Cell **11:** 747–763.